applied sciences

MDPI

Article

Study of Partial Discharge Inception Voltage in Inverter Fed Electric Motor Insulation Systems

Leire Elorza Azpiazu *, Gaizka Almandoz, Aritz Egea, Gaizka Ugalde and Xabier Badiola

Faculty of Engineering, Mondragon Unibertsitatea, 20500 Arrasate-Mondragón, Spain
* Correspondence: lelorza@mondragon.edu

Abstract: This article performs a thorough evaluation of different environmental and electrical waveform characteristics affecting PDIV on electric motor winding insulation. Temperature received special attention, as it clearly affects PDIV. Additionally, the PDIV models found in the literature were reviewed. Considering that the winding of the electric motor can reach 180 °C during operation, the experiments were performed at high temperatures in order to evaluate the performance of PDIV models. Several models were studied regarding their accuracy at high temperatures and the advantages and disadvantages of each one were identified. Based on the analysis, a simple analytical model to estimate the PDIV of twisted pairs depending on the temperature was proposed. All in all, the proposed model was the best compromise between computational requirements and PDIV estimation accuracy at high temperatures. Finally, future lines were identified. Further studies are necessary that consider the humidity, rise time, and pulse width effect on PDIV. Moreover, new models regarding both, environmental and waveform characteristics are necessary to accurately estimate PDIV. Extended volume–time theory seems to be a good basis for that.

Keywords: electric motors; electric motor insulation; insulation degradation; Partial Discharge (PD); Partial Discharge Inception Voltage (PDIV); electrical stress; environmental stress; PDIV model

Citation: Elorza Azpiazu, L.; Almandoz, G.; Egea, A.; Ugalde, G.; Badiola, X. Study of Partial Discharge Inception Voltage in Inverter Fed Electric Motor Insulation Systems. *Appl. Sci.* **2023**, *13*, 2417. https://doi.org/10.3390/app13042417

Academic Editor: Loránd Szabó

Received: 20 December 2022
Revised: 7 February 2023
Accepted: 8 February 2023
Published: 13 February 2023

1. Introduction

Nowadays, the interurban and urban mobility of people worldwide is mainly based on internal combustion engine vehicles. Social awareness of climate change and pollution in the urban environment, however, has led to electric and hybrid vehicles becoming increasingly important [1]. In electric vehicles (EV), maximising autonomy is a key factor, which requires high power density drives. Thus, the volume and weight of the traction system must be minimised, while maintaining high efficiency levels [2].

In recent years, new power electronic technologies based on Wide-bandgap devices (WBG) of gallium nitride (GaN) and silicon carbide (SiC) have caused it to be possible to increase the switching frequency with high efficiency, leading to more compact converters [3]. Additionally, by increasing the switching frequency, it is possible to increase the speed of the electric machine. This way, for the same mechanical power, the torque requirement and, therefore, the size of the machine can be reduced. Hence, with the use of electric machines fed by WBG converters, both, the power converter and electric machine can be reduced in size and weight, maximising the autonomy of the EV [4]. In this line, SiC MOSFETs and GaN HEMTs are already being introduced to electromobility [5,6].

This application, however, introduces new challenges, where several are associated with the insulation of the motor windings [7]. WBG devices can generate short rise and fall time voltage pulses, which amounts to a higher dv/dt than conventional Si technology converters. Several investigations have shown that high dv/dt voltage pulses can lead to, on the one hand, unequal voltage distribution within the motor winding [8,9] and, on the other hand, overvoltages up to two times the DC-link voltage, due to reflected wave phenomena [10,11]. Both effects are commonly known as electrical stress factors

for winding insulation and can cause partial discharge (PD) activity, being one of the most common fault factors in winding insulation [12]. In particular, turn-to-turn winding insulation (considered the weakest point of the winding insulation system) is most affected by PD deterioration [7,13,14].

In order to protect the insulation from the issues caused by WBG converters, different solutions are proposed in the literature. A possible solution is the use of filters to reduce the dv/dt [15]. Additionally, the use of multi-level inverters was also shown to lengthen the lifetime of the insulation due to the reduction in PD amplitude [16]. Even using these solutions, in the case of the insulation being exposed to higher electric stress than expected and reaching partial discharge inception voltage (PDIV), a PD event will probably occur and the deterioration of the insulation system will be accelerated [14,17–19]. In addition to electrical factors, environmental factors may enhance PD activity and, therefore, insulation deterioration. For the same application and waveform characteristics, depending on the surrounding conditions, PD events can appear or not, due to their influence on PDIV [20].

It is known that during service, PDIV decreases because of the mentioned electrical and environmental factors [21–24]. When the PDIV reaches the operation voltage, there might be constant PD activity. This will result in even faster deterioration and a probable insulation breakdown. Thus, the aim of the insulation design should be to ensure that PD-free service lasts as long as possible. For that, it is important to have a margin between the initial PDIV and operating voltage. The higher this margin is, the longer the time required for the degradation to have a PDIV equal to the operating voltage. Therefore, the PDIV of the turn-to-turn insulation is a key factor in the design of the insulation system. Accurate models for PDIV estimation regarding different operation factors are necessary. Although mechanical factors can also be stress factors, they are not easy to consider. These factors, such as vibrations, may cause defects on the insulation surface, which are difficult to examine and replicate.

The present article has two main objectives. First, to summarize from the existing literature how WBG-derived electrical factors (such as waveform and polarity, frequency, rise time and pulse width), and environmental factors (pressure, temperature, and relative humidity) affect PDIV. Mechanical factors are not considered in this study. Second, to analyse whether it is possible to accurately predict the PDIV value considering the analysed factors. This is intended to offer guidelines for the insulation design process, focusing on turn-to-turn insulation. For that, the main variables affecting PDIV are reviewed from the literature. Additionally, the effect of temperature on PDIV is discussed based on experimental results. Then, different models proposed in the bibliography are studied regarding their performance at high temperature. The advantages and disadvantages of each model are also exposed. Additionally, a new model is proposed, where experiments and FEM simulations are avoided. Finally, some guidelines are proposed according to the PDIV estimation. The contributions of this article include: (1) a comprehensive analysis of the electrical and environmental variables affecting PDIV, (2) the study of the accuracy of different models proposed in the literature for estimating the behaviour of PDIV, and (3) a proposal of an improved PDIV model considering temperature conditions.

This article proceeds as follows. First, Section 2 develops a comprehensive literature review of several electrical and environmental variables affecting PDIV. Different models predicting PDIV are also gathered. Section 3 introduces the experimental layout, test procedure, and sample materials for PDIV measurements at different temperatures. In Section 4, the effect of temperature in PDIV is analysed. Additionally, the performances of different modelling techniques regarding temperature are compared and a new model is proposed. The experiments are developed to perform the studies in Section 4. Section 5 is a discussion of the technological gaps identified regarding variables affecting the PDIV and modelling. Finally, Section 6 concludes this article.

2. Literature Review

2.1. Variables Affecting PDIV

Different variables affecting PDIV are identified and gathered in this section. On the one hand are environmental conditions, such as pressure, humidity, and temperature. On the other hand are electrical factors derived from WBG converters (waveform and polarity, frequency, rise time, and pulse width). Finally, the main points of how each variable affects PDIV are collected.

2.1.1. Environmental Conditions

Two principal factors affecting PDIV are the surrounding air properties and enamel properties of the sample. Both of them might be influenced by environmental factors. In the following sections, the effect of pressure, relative humidity (RH), and temperature on PDIV/RPDIV (repetitive partial discharge inception voltage) are gathered. The RPDIV is the minimum peak-to-peak impulse voltage at which more than five PD pulses occur on ten voltage impulses of the same polarity according to IEC 60034-18-41 [10].

Pressure

The pressure principally affects the PDIV due to its influence on the air breakdown voltage. As described in Paschen's law (explained in Section 2.2), the breakdown voltage for a given gas (air) and electrode material can be defined as a function of the product of the gas pressure and the gap distance [25]. The PDIV is the minimum voltage at which the voltage across the air gap is equal to the breakdown voltage of the air. Therefore, the surrounding air pressure has a significant effect on the PDIV.

Several investigations showed that the evolution of the PDIV has a *U* shape with an increase in pressure. L. Lusuardi et al. [26] measured the PDIV of twisted pairs with a 50 Hz sinusoidal waveform. Starting at 5 mbar, the authors detected that the PDIV decreased until the minimum was reached at 50–70 mbar. Then, it increased with the increase in pressure, creating the aforementioned *U* shape.

In addition, C. Abadie et al. [27] note that the increase in pressure in from 100 to 1013 mbar increases the PDIV for twisted pairs. D. Meyer et al. [28] obtained the same influence of the pressure in a range of 200–1000 mbar on RPDIV. The results reported in the mentioned studies [26–28] are compared in Figure 1. The PDIV results are normalised to 1000/1013 mbar and are depicted in a pressure range from 5 to 1013 mbar. In this case, the characteristic *U* shape is only seen in the results from [26], as the minimum PDIV value is at around 50–70 mbar and [27,28] measured above this pressure.

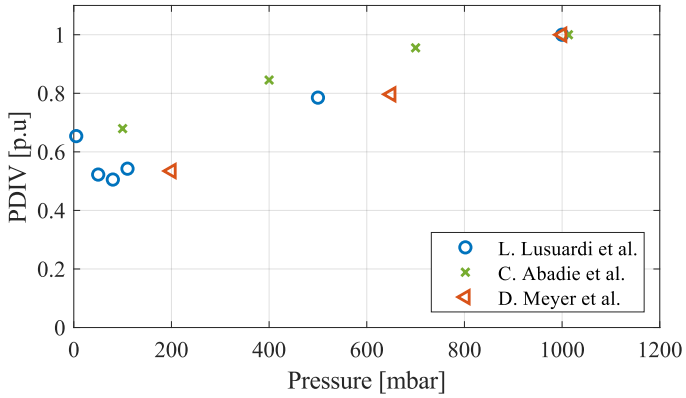

Figure 1. Comparison of the dependence of PDIV on pressure (L. Lusuardi et al. [26], D. Meyer et al. [28], and Abadie et al. [27]).

To sum up, starting at a low pressure, the PDIV is inversely affected by the pressure until it reaches a minimum, followed by an increasing proportional tendency, leading to a *U*-shaped evolution.

Humidity

Regarding the humidity, both air and enamel properties are affected. According to M. Fenger and G. Stone [29] (at 25 and 50 °C, RH 10–90% and PDIV values above 5000 V), the PDIV increases with increasing humidity until a peak value is reached. Afterward, the PDIV decreases with an increase in the humidity. Therefore, they suggest that the PDIV is affected by two mechanisms, the aforementioned air properties and enamel properties. The peak value of PDIV relates to the point at which the effect of the first mechanism is neutralised by the second mechanism (critical RH [20]). Similarly, F. Guastavino et al. [20] noticed the same effect on voltage levels above 5300 V at 23 °C in a range of RH 35–80%.

According to the first mechanism, before the peak PDIV value, a proportional relationship between the humidity and PDIV is seen, due to the increase in air breakdown voltage. When the moisture content is increased (an increase in RH), the electric breakdown strength of the air is increased. This observation is in good agreement with [30]. The author explains that the breakdown voltage of the humid air is increased with the increase in RH from 0% (dry air) to 40%. The water vapour has a higher breakdown strength than air, therefore, the mixture of water vapour and air (higher RH) has a higher breakdown voltage. Additionally, the authors of [20] observed that, in this range, when decreasing the RH, the area of PD activity is concentrated in a small area, deteriorating the enamel more. Even though no PDIV is studied, reducing the area will result in a lower PD activity probability and the PDIV will be defined by a higher voltage level [31].

The second mechanism, however, creates an inverse relationship between the PDIV and humidity. When RH is increased, the condensation of water on the insulation can enhance the electric field. D. Fabiani et al. [32] measured an increased space charge in the bulk of polymers with nanocomposite fillers. The same author observed in [33] that the space charge accumulated in the insulation bulk often has often the same polarity as the injecting electrode (e.g., a positive charge accumulation near the positive electrode). This increases the overall electric field in the air gap. Consequently, the PDIV is defined by a lower voltage value. Similarly, F. Guastavino et al. [20] mentioned that PD activity might also be affected by the RH.

Other investigations suggested that the relative and imaginary part of permittivity increase with humidity, which decreases the PDIV as well [34,35]. Y. Kikuchi et al. [35] analysed the electric field strength in the air gap (E_{gap}), taking into account the relative permittivity (ϵ_r) using a plane capacitor model (Equation (1), with d_{air} being the gap length and t_{ins} the insulation layer thickness). The electric field intensity increases with the relative permittivity and, therefore, the RH. However, based on optical emission spectroscopy (OES) measurements, the author concluded that not only the increase of ε_r of the enamel wire increases the E_{gap} but also other mechanisms (not specified).

$$E_{gap} = \frac{V}{d_{air} + 2t_{ins}/\varepsilon_r} \quad (1)$$

For lower voltage values (<3450 V), F. Guastavino et al. [20] defined the critical RH value below the analysed RH range (35–80%). This suggests that the second mechanism is apparently dominant in the whole range of humidity for low voltage. This agrees with the observation of several authors at lower voltage levels at room temperature (25 °C) [35–38], 60 °C [35], 80 °C [35], and 90 °C [39]. W. Hassan et al. [39], on the contrary, noted at 30 °C an increase in the PDIV with an increase in RH. This is explained by the surface discharge predominating, due to the semiconductive layer generated in the insulation with the interaction between moisture and byproducts formed at PD. Therefore, the influence of the RH depends on the exposure temperature. Moreover, D. Muto et al. [38] concluded that, after washing the samples with pure water, there was no effect of humidity on PDIV in a range of 50–95%. In this case, the decreasing effect of the PDIV (in samples before washing) was due to a change in surface conductivity because of contaminant (Na,

K, Cl, etc.) adhesion with touching by bare hands, which indicates that the other impact factors considered previously are negligible.

To summarise, generally speaking, two main mechanisms result from an increase in the relative humidity. At low RH values, the PDIV increases with the increase in the RH due to the increase in the air breakdown strength and decrease in the PD activity surface, until a peak PDIV value is reached. Then, the PDIV is inversely affected by the RH. The increase in the space charge accumulation in insulation bulk and relative and imaginary part of permittivity, resulting from the increase in RH, decreases the PDIV. At high voltage levels (>5300 V), both mechanisms could be developed, whereas, at low voltage levels (<3450 V), the second mechanism is predominant. Even so, some authors found an inverse effect of conductivity on PDIV, or no effect of RH, if samples cleaned with pure water are measured. Further investigation is necessary, considering the voltage level, temperature, and cleanness of the samples when the RH effect on PDIV is studied.

Temperature

As in the case of humidity, temperature impacts both air properties and insulation properties. Referring to the former, an increase in temperature inversely affects the air density, decreasing the electric breakdown strength of air [38,40]. Additionally, W. Hassan et al. [39] and L. Lusuardi et al. [26] explain that the electron mean free path is increased with a decrease in air density. Consequently, electrons gain more energy and generate electric discharges by crossing a greater distance between collisions [39]. As a result, an increase in temperature decreases the PDIV [26,38–41].

Moving to the insulation properties, D. Muto et al. [38] observed that an increase in relative permittivity with temperature (in the range 25–230 °C) decreased the PDIV. Different insulation materials (Polyamide-imide (PAI) and Polyetheretherketone (PEEK)) with different permittivity–temperature relationships that (increase the relative permittivity with temperature) are analysed. It is shown that not only are changes in air density dominant but also the evolution of permittivity with temperature must be considered. These conclusions are in good agreement with [42]. It must be kept in mind that, depending on the material, the relative permittivity can increase or decrease with temperature. Therefore, depending on the relative permittivity evolution, the PDIV will increase or decrease with the temperature. On the contrary, L. Lusuardi et al. [26] did not notice a considerable dependency on PAI in the range of 25–140 °C. They explained that the analysed temperature is well below the glass transition temperature (275 °C), so the dependency of the relative permittivity on the temperature is limited. In insulation materials with lower glass temperatures, the temperature dependency could be enhanced.

Considering these studies, it is clear that there is an inverse relationship between temperature and PDIV due to air electric breakdown voltage decrease. However, in view of relative permittivity, the PDIV evolution can be analogous or inverse to the temperature. Thus, when the relative permittivity decreases with the temperature, both factors, air and permittivity, have an opposite effect on the PDIV. In this case, it is necessary to decide whether air properties or relative permittivity is the predominant factor to define the evolution of the PDIV with temperature.

2.1.2. Electrical Factors

In the following sections, the effect of the main electrical waveform properties on the PDIV is discussed: waveform and polarity, frequency, rise time, and pulse width. The conditions necessary to develop PD activity are two key factors for the comprehension of the following sections: (1) the applied voltage must be higher than the ignition/inception voltage and (2) a free electron should be available [26] or a critical number of electrons should be reached [43]. It is worth mentioning that, when the following lines refer to a free electron, the Townsend discharge mechanism is considered. When a critical number of electrons is mentioned, the Streamer mechanism is considered. The differentiation is

based on what the author of the corresponding article uses. More information regarding the Townsend and Streamer mechanisms is provided in Section 2.2.1.

Waveform and Polarity

The differences between the use of sinusoidal and square waveforms, either unipolar or bipolar, to define the PDIV of twisted pairs have been studied by different authors. It is worth mentioning that, in the studied cases, the PDIV is defined by increasing the voltage at a constant rate until the PD activity is detected. In [26], after observing PDIV experimental data for sinusoidal and bipolar square waveforms, it is concluded that only the peak value of the applied voltage is important for the definition of the PDIV, whereas the waveform does not affect the PDIV. It is explained that an error in the definition of the PDIV could arise when measuring using impulse bipolar voltages due to overshooting. Figure 2 depicts a situation where the peak voltage exceeds the ignition voltage (V_{inc}) and the PD could happen in any voltage level of the overshoot, as long as there is a free electron available to start the avalanche.

Two different cases are distinguished for the definition of PDIV. (1) If the peak voltage of the waveform is defined as PDIV, a higher value than the inception voltage could be considered, resulting in a positive error. (2) If the DC voltage is defined as the PDIV, as the DC voltage is lower than the ignition voltage, a negative error arises. The error in the definition of the PDIV considering either peak or DC voltage is enhanced with a larger overshoot. This could also happen in sinusoidal waveforms; the author remarks that, due to its low derivative at 50/60 Hz (generally used), this error could be neglected. The authors of [33,44] came to the same conclusion after measuring the PDIV for sinusoidal and repetitive impulse waveforms.

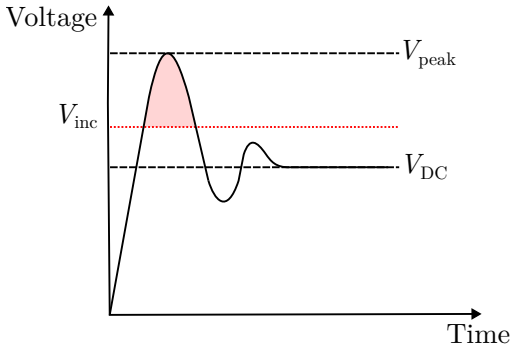

Figure 2. Sketch of PD inception using impulse voltages with overshoot. Image based on [26].

In addition to the waveform, D. Fabiani et al. [33] compared the PDIV for unipolar and bipolar square impulses. It was observed that the PDIV value measured using the unipolar waveform is around double that measured with the bipolar waveform, which also suggests that PDIV depends on the peak-to-peak value of the applied voltage. Finally, observing the influence of the polarity in the PDIV measurements using unipolar waveform, the author of [45] shows that the polarity has little impact on the PDIV measurements under unipolar voltages in twisted pairs. In fact, no polarity dependence is expected for twisted pairs because of the symmetry of the electrode configuration.

It is of particular interest that, under a unipolar waveform, there is a considerable space charge (in the insulation bulk) and surface charge (in the insulation surface) accumulation compared to a bipolar waveform (either sinusoidal or square). D. Fabiani et al. [33] exposed twisted pairs to unipolar and bipolar waveforms with a 0.5 PDIV voltage level at 50 Hz. The PDIV is measured at different exposure times (defined as the poling time). It is shown that, for a unipolar waveform, the PDIV value increases and then decreases. The increase in the PDIV at the initial stage is due to the surface charge accumulation. The accumulated charge generates an internal electric field in the opposite direction of the applied field. This way, the overall electric field in the air gap is reduced, consequently increasing the

PDIV. The latter decrease in the PDIV during the poling time is related to the insulation bulk charge (Section 2.1.1), which prevails during the time. In a bipolar waveform, there is no effect on the PDIV, since very small charge accumulation is noticed in the insulation bulk and surface. This phenomenon is also known as the memory effect. According to several authors, the memory effect can influence the PDIV and RPDIV when consecutive measurements are collected [41,43].

Recapitulating, the PDIV is not affected by the waveform (bipolar or unipolar) and polarity (negative or positive), but the peak-to-peak applied voltage value is the main factor that defines the PDIV. Nonetheless, the waveform and polarity can affect the space charge accumulation if the sample is subjected to PD for a prolonged time, which has an effect on the PDIV. Hence, the memory effect must be considered in consecutive PDIV measurements.

Switching Frequency

Different conclusions are obtained regarding the effect of the switching frequency on the inception voltage. On the one hand, in [26,46] it is stated that, for a square waveform with constant rise time (8 ns), the PDIV is independent of the switching frequency in the range of 10–100 kHz as long as the real permittivity of the insulation material is as well. If real permittivity depends on the frequency, above a critical frequency, which depends on the material, the dipole orientation will not occur, resulting in a dielectric loss peak and a decrease in the real permittivity. This could increase the PDIV [38]. Moreover, the heat generated by dielectric losses could increase the temperature, reducing the air density and, therefore, the PDIV. As a result, in case the fundamental frequency and the harmonic distribution of the waveform are above the mentioned critical frequency, the PDIV could be affected by the switching frequency.

Z. Wei et al. [47] came to the same conclusion. They detected that the PDIV slightly increases by about 6% with an increase in the frequency in the range of 1–10 kHz for a square waveform with a fixed rise time (100 ns) and duty cycle (tested at 0.2, 0.5, and 0.8 duty cycles). Nonetheless, they assumed that the effect of the frequency on the PDIV is negligible. S. Matsumoto et al. [37] did not perceive any effect of the frequency on PDIV in a range of 20–200 kHz for sinusoidal waveforms at different humidity conditions.

On the other hand, several authors confirmed that the frequency (2–2000 Hz) can affect the PDIV if a repetitive waveform is considered, that is to say, RPDIV. In [48,49], it is mentioned that the larger the frequency, the stronger the influence of charges left by the previous discharge (i.e., less time to relieve the charge). This could help the extraction of electrons, leading to the discharge occurring at a lower voltage level since the time lag (the time necessary to generate a free electron once the ignition voltage is reached) is reduced [50]. The increase in free electrons due to the charge accumulation is presented in discharges occurring in the same half-cycle (homo-discharges) [51]. The RPDIV follows the definition of homo-discharge, as subsequent PDs in the same half cycle are necessary. This is demonstrated in [52], where PD patterns are shown for 100 Hz and 1 kHz. For high frequency, charge promotes PD events reaching high PD magnitudes, whereas, at low frequency, the PD magnitudes are lower, especially in the positive flank, due to the absence of a charge. Additionally, S. Akram et al. [19] conducted PD experiments under repetitive impulse voltages at higher voltage values than PDIV. The authors observed that, for higher frequencies, the PD activity was triggered earlier during the rising edge. It is concluded that this effect is caused by the charge accumulation left by the previous discharges, similar to [48,49].

Similarly, in [28,53], it is observed that, for unipolar PWM waveform, the RPDIV (defined by the peak-to-peak impulse voltage) decreases with an increase in the switching frequency in the range of 20–200 kHz, being stabilised at around 75–100 kHz. It is mentioned that, above 10 kHz, the memory effect can be considered perfect, so its effect at higher frequencies should be constant. Aside from the charge accumulation, these researchers studied two main factors to explain this effect, the relative permittivity of the insulation and the oscillation of the wave forms in the frequency range used. After measuring the relative permittivity at different

frequencies, they concluded that its variation is not considerable enough to have an effect on the RPDIV. Alternatively, they examined the instantaneous frequency spectrum of the pulse. They found that the largest frequency content corresponds to the overvoltage and does not change for different switching frequencies. Consequently, they confirmed that the RPDIV is not dependent on the different instantaneous frequency contents of the applied voltage overvoltage. Finally, they concluded that the average amplitude of the overvoltage changed with the increase in the frequency, even maintaining the peak voltage. Thus, the probability of developing the PD is higher and the RPDIV can be detected in lower voltage levels at increasing voltage tests (generally used to determine PDIV and RPDIV).

To summarise, the PDIV is not affected by the switching frequency, as it is defined when the first PD is developed. The RPDIV, however, is affected by the enhancement of free electrons due to charge accumulation at frequencies below 10 kHz, which decreases the RPDIV. Moreover, the overshoot average amplitude also increases the probability of developing the PD in switching frequencies up to 75–100 kHz. Finally, over 100 kHz, the RPDIV tends to stabilise.

Rise Time

There is no agreement about the effect of the rise time on the PDIV in the literature. There are two main conclusions: (1) the PDIV is not affected by the rise time, but by the overshoot and its characteristics, which are enhanced at low rise times. (2) The PDIV is decreased with a decrease in the rise time when there is an absence or low overshoot.

Referring to conclusion (1), several authors agree that the rise time does not affect the PDIV, but the overshoot resulting from the low rise time used in WBG devices is the main factor affecting the PDIV [26,45,46,52,54]. Therefore, different results are obtained depending on whether the PDIV definition is determined by selecting DC voltage or peak voltage (explained in Figure 2). The results reported in the literature for PDIV peak and PDIV DC are summarised in Figure 3. The PDIV values are normalised to the highest rise time (which is also the lowest overshoot) in each study.

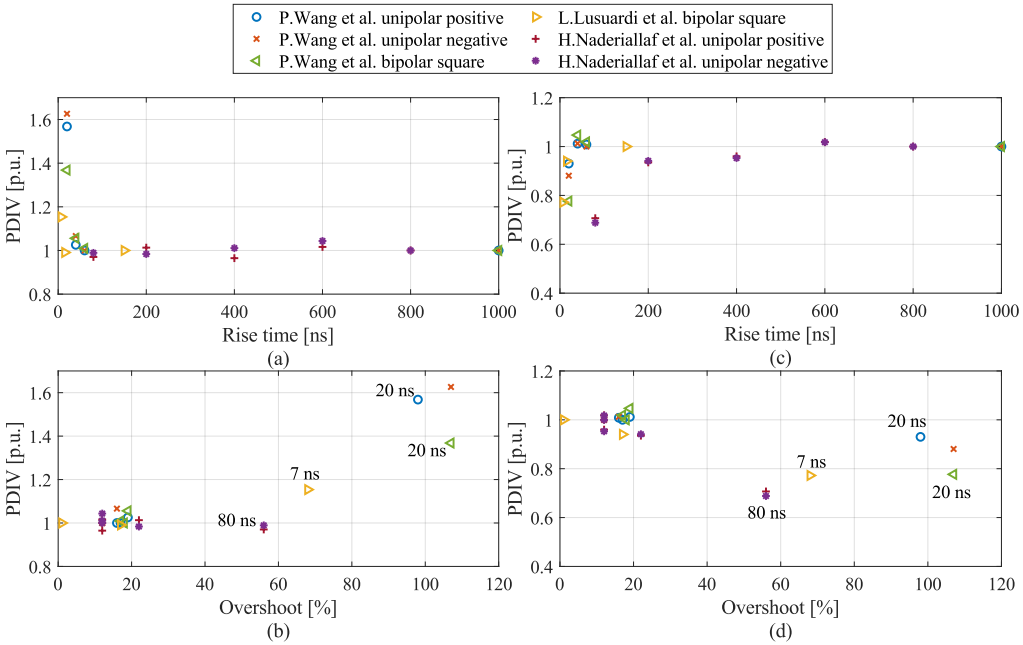

Figure 3. Bibliography results (P.Wang et al. [45], L. Lusuardi et al. [26], and H. Naderiallaf et al. [54]) of (**a**) PDIV peak vs. rise time; (**b**) PDIV DC vs. rise time; (**c**) PDIV peak vs. overshoot; (**d**) PDIV DC vs. overshoot.

In Figure 3 the, peak and DC PDIV are collected depending on the rise time and overshoot percentage. Focusing on Figure 3a, it can be seen that, independent of the waveform and

its polarity (bipolar or unipolar positive and negative), for a rise time above 20 ns, constant peak PDIV values were obtained. On the contrary, for lower rise times, there was a general increasing effect. For some researchers, this inflexion point was below 20 ns [45], whereas for others it was below 15 ns [26]. Moving to Figure 3b, the DC PDIV showed a similar effect but with a decreasing tendency. The change from a constant to an increasing/decreasing effect of the PDIV comes with a considerable increase in overvoltage. The relationship between the PDIV and the overshoot is depicted in Figure 3c,d. At low overshoots, there is no considerable effect on the peak and DC PDIV, as there is at high overshoots, which correspond to 7 ns [26], 20 ns, [45] and 80 ns [54] rise times.

Figure 4 summarises the relationship between the peak and DC PDIV, depending on the overshoot. A linear relationship is evident. The difference between the peak and DC PDIV value increased with the waveform overshoot.

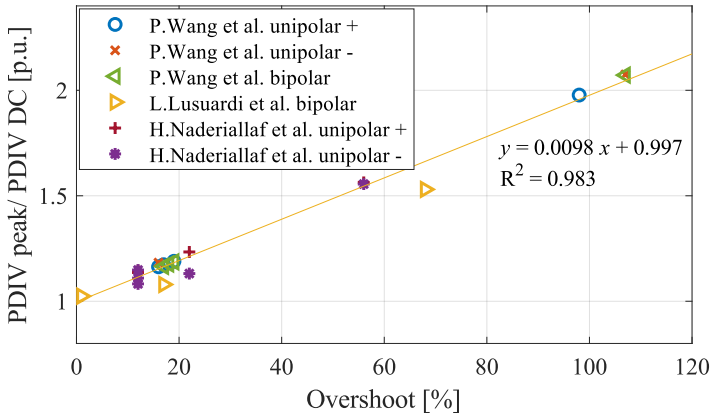

Figure 4. Relationship between PDIV peak and DC as a function of the voltage overshoot based on the literature results (P.Wang et al. [45], L. Lusuardi et al. [26], and H. Naderiallaf et al. [54]).

After observing the impact of overshoot on the PDIV, N. Hayakawa et al. [31] proposed an extended volume–time theory based on the Streamer discharge mechanism, which deals with the generation probability of starting electrons considering temporal and spacing changes in electric field distribution (Section 2.2.4). With this theory, the PDIV can be discussed as the sum of starting electrons generated and is defined as the voltage level where the generation probability exceeds 50%. Accordingly, with surge voltages, the available starting electrons' quantity is the dominant factor used to define the PDIV. Several waveforms with rise times between 60 and 3000 ns and overshoot between 150% and 180% are analysed in [31] to validate the theory. It is worth mentioning that the highest overshoot corresponds to the lowest rise time, whereas the lowest overshoot corresponds to the highest rise time. It is noticed that peak PDIV increases with high overshoot, similar to in the previously mentioned studies [26,45,54]. In this case, however, peak PDIV is further increased for lower rise times, despite having a similar overshoot of higher rise time waveforms. It can be said that not only does the overshoot level influence the peak PDIV, but also the rise time. For the same peak voltage level, the higher the rise time, the higher the discharge generation probability. The time the voltage is maintained above the inception value is higher, increasing the starting electron availability. Hence, the studies concluded that the PDIV increases with a decrease in rise time due to the characteristics in the time range of the inverter surge voltage.

Moving to conclusion (2), several authors conducted PDIV measurements without or with an inconsiderable overshoot (<10%) in order to separate the impact of the rise time from the overshoot [43,47]. Z. Wei et al. [47] showed that the PDIV (measured in peak) is reduced by 28% if a square unipolar positive voltage with a rise time of 150 ns is used instead of a 60 Hz sinusoidal waveform. Moreover, by decreasing the rise time from 150 ns to 60 ns, the PDIV is decreased by 21%. The study concluded that the AC PD test does not correctly evaluate the insulation capability of electrical apparatus subjected to

impulse voltage stress. Similarly, the authors of [43] stated that the DC PDIV decreases by 23–38% when the rise time of a unipolar waveform is decreased from 1000 ns to 150 ns. However, its influence is not so evident in the rise time range 100–150 ns. In [26], a low rise time bipolar square waveform without overshoot (150 ns and 1%, respectively) measuring the PDIV (measured in peak and DC) results were compared with sinusoidal waveform measurements; these were found to have a negligible difference. Hence, it supports using sinusoidal waveforms to test the winding insulation.

To explain how the rise time influences PDIV, the authors of [43] observed, based on the extended volume–time theory, that for different rise times, the number of electrons (N_0) necessary for PD to happen is stable. For a fixed pulse width, with a shorter rise time, the electron generation can start earlier, as long as the applied voltage exceeds the inception voltage. However, it must also be considered as the initial electron generation rate in the air gap and the enamel surface, which depends on the electric field. As shown in [31], the electron generation rate from the air gap and enamel surface is increased with an increase in electric field intensity and as a result of applied voltage. Moreover, the author of [43] mentions that, under different rise times, the space charge influencing the electric field may be different and could influence the electron generation rate. Therefore, not only the rise time but also the electron generation rate are important factors for the PDIV in waveforms without overshoot.

Based on the theoretical explanations provided by the authors of [43], a simplified schematic representation is depicted in Figure 5. For a fixed pulse width, two rise times are represented. For a lower rise time, the ignition voltage is reached earlier and electron generation starts earlier (t_{0l}). The electrons have enough time to reach a critical value and develop the PD activity. On the contrary, for a higher rise time, in addition to a later electron generation starting (t_{0h}), the generation rate is slower and, therefore, by the time critical N_0 is achieved, the applied voltage can be at a lower level than at inception, thereby avoiding PD, and the PDIV can be set to a higher voltage level.

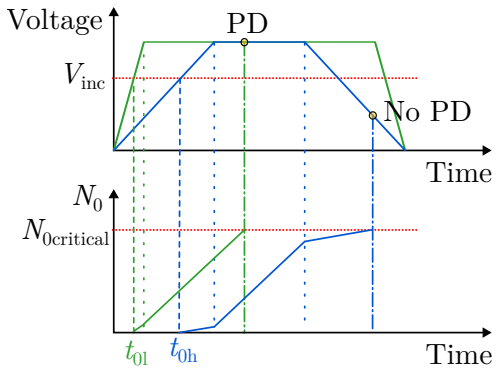

Figure 5. Simplified sketch of the effect of rise time on PDIV.

Overall, when the PDIV is measured with high overshoot, the main factor influencing it is the overshoot level rather than the rise time. In this case, it is not possible to correctly measure the ignition voltage as error results if the peak or DC value of the applied voltage is considered as the PDIV. Higher overvoltage will result in higher error results. However, if the measurement is carried out without overshoot, there is no consistent answer in the literature. Considering that the rise time influences the PDIV, with a lower rise time, the initial electron generation starts earlier (as long as ignition voltage is overcome) and a lower voltage is sufficient to achieve PD, resulting in a lower PDIV value (even considering peak or DC applied voltage values).

Pulse Width

Generally speaking, researchers agree that a longer pulse width increases the probability of a starting electron occurring, as long as the applied voltage is maintained above the inception voltage. Once the ignition voltage is reached, if the pulse is maintained for a long time, there is more time to obtain a critical initial electron number, favouring PD

activity [48]. However, the effect of the pulse width on the measurement and definition of the PDIV is not so clear.

Some authors state that the PDIV is not dependent on the pulse width as long as the rise time is sufficiently high [52]. Cavallini et al. [52] concluded that there is no effect on the PDIV for unipolar 50 Hz and 300 ns rise time pulse in a range of 0.5–50 µs pulse width. This is similar to in [54], where it is perceived as having an almost constant but slightly increasing effect on the PDIV with a pulse width for unipolar (positive and negative) 2.5 kHz and a 160 ns rise time pulse in a pulse width range of 40–100 µs (duty rate 10–25%). The slight difference in the results is mainly related to the measurement uncertainty. At a lower pulse width, the variance of the results is higher, due to the higher impact of the firing electron delay.

On the contrary, Wei et al. [43] noticed a dependency of the PDIV on pulse width, with a 1000 ns rise time for unipolar waveform (1–100 kHz). They came to the conclusion that the PDIV is reduced with an increase in the pulse width (2–800 µs), following, approximately, an inverse power law. The authors deduced that, for a defined rise time, the number of initial electrons was maintained for different pulse widths. For a longer pulse width, the electrons can be generated within a longer period (as long as the applied voltage is higher than the ignition voltage), and a lower applied voltage is enough to reach the necessary number of electrons to derive a PD. Therefore, the increase in the pulse width decreases the PDIV, with a smaller effect for longer pulse widths. Similar results are presented for formed wound samples [55] and plate-point analysis [56].

Considering lower rise times, Wei et al. [43] also observed the same tendency that they observed for higher rise times (1000 ns) in the range of a 100–150 ns rise times. However, with a 70 ns rise time, L. Benmamas et al. [57] identified an increasing effect of PDIV (9%), with a pulse width in the range of 1000–9000 µs for unipolar 100 Hz waveforms. The authors explained that the increase in PDIV is mainly related to a decrease in the nonconduction duration (when the voltage is 0 V) over a period of time (9000 and 1000 µs nonconducting duration for 1000 and 9000 µs pulse widths, respectively). The application of the voltage generates the displacement of the surface charges, creating an electric field in opposition to the applied electric field and reducing the total electric field. During nonconduction periods, these charges are redistributed. When the nonconducting time slot is low compared to the exposure time, only a fraction of charges are redistributed, resulting in a charge accumulation, which decreases the total electric field. The PDIV can be defined at a higher voltage level (the case of 9000 µs pulse width and 1000 µs nonconducting duration). When the authors developed the same analysis with a 1 kHz waveform (pulse width 100–900 µs), the influence of the pulse width on the PDIV was reduced. In these cases, the nonconducting duration was higher than the pulse width, leading to a lower influence of the charge accumulation between consequent pulse widths. This would agree with the results reported in [52,54] as the nonconducting interval of the different pulses are high compared to the voltage exposure so that the resulting PDIV remains practically constant. It has to be mentioned that, in [57], the variance of the measurements is high and the maximum difference of the PDIV with a duty cycle is not higher than 10%.

To sum up, a higher pulse width enhances the PD appearance, as there is enough time to achieve the critical initial electron number. However, the influence of the pulse width on the PDIV is not clear. For high rise times, the effect of the pulse width appears to be negligible, as the critical initial electron number is reached during rising. For lower rise times, the authors of [43] stated that the pulse width decreases the PDIV, assuming that there is more time to reach the electron number. Other researchers concluded that the PDIV increases if the nonconduction duration is short compared to the exposure time (pulse width) due to charge accumulation.

2.1.3. Summary of Variables Affecting PDIV

Several investigations regarding the effect of environmental conditions and electric variables on PDIV definition are summarised in Table 1. The most relevant variables are

summarised and the effect of an increase in each variable on the PDIV is categorised as increase, decrease, or negligible. The measuring conditions are specified only in the cases that they are considered relevant. For instance, the differences in the effect of humidity on high and low voltage levels.

Table 1. Summary of variables affecting PDIV.

Affecting Variable	Effect on PDIV	Range	Measuring Conditions	Reason	Notes	Ref.
Pressure	Decrease	5–50/70 mbar	-	↓ air breakdown V	Range depends on air gap and material	[26]
	Increase	100–1013 mbar	-	↑ air breakdown V		[26–28]
Humidity	Decrease	>50%	$V \leq 5$ kV $T_{amb} \leq 50$ °C	↑ insulation permittivity and bulk space charge	-	[20,29,34]
		10–97%	$V \leq 3.5$ kV T_{amb} = 25, 90 °C			[20,36–39]
	Increase	<50%	$V \geq 5$ kV $T_{amb} \leq 50$ °C	↑ air breakdown V, ↓ area of PD activity	-	[20,29]
		50–97%	$V \leq 3.5$ kV T_{amb} = 30 °C	Surface discharge more prominent than internal		[39]
	Negligible	50–95%	$V \leq 3.5$ kV T_{amb} = 25 °C Pure water washing	PDIV dependency due to bare hand contaminants	-	[38]
Temperature	Decrease	25–230 °C	-	↓ air breakdown V and change of permittivity		[26,38–40]
Waveform and polarity	Negligible	Sinusoidal	-	It is defined by peak-to-peak applied voltage	Under absence of overshoot	[26,33,44]
		Bipolar square			After prolonged PD exposition PDIV increased by memory effect	[26,33,44]
		Unipolar square +/−			Consecutive PDIV measurements increased by memory effect	[26,33,44]
Switching frequency	Decrease *	2–10,000 Hz	-	↑ space charge due to homo-discharge memory effect	-	[48,49,52]
		10–75 kHz		↑ average amplitude of overvoltage		[28,53]
	Negligible	1–200 kHz	-	No memory effect on the detection of first PD	If permittivity of the insulation is independent on frequency	[26,37,46,47]
Rise time	Increase	60–1000 ns	No overshoot	↓ time for initial electron generation	-	[43,47]
	Negligible	7–1000 ns	Overshoot in low rise time waveforms	Resulting from overshoot rather than rise time	-	[26,45,46,52,54]
		150 ns	No overshoot		Compared to 60 Hz sinusoidal	[26,46]
Pulse width	Decrease	2–800 µs	Rise time 100–1000 ns	↑ time for initial electron generation	Change frequency and duty rate	[43,55,56]
	Increase	1000–9000 µs	Rise time 70 ns, 100 Hz	non-conducting duration > conducting time	Same frequency, change duty rate	[57]
	Negligible	0.5–100 µs	Rise time > 160 ns	Critical initial electron number during rising edge	Same frequency, change of duty rate	[52,54,57]
		100–900 µs	Rise time 70 ns, 1 kHz	Non-conducting time > conducting time		[57]

* for RPDIV.

2.2. PDIV Modelling

With the purpose of ensuring that PD-free service lasts as long as possible, it is crucial to consider the PDIV during the preliminary design stage of the insulation system. As previously mentioned, the turn-to-turn insulation is the weakest point of the insulation system and has a higher probability of developing PD activity. Therefore, to design an insulation system adapted to the application preventing PD, it is necessary to develop accurate models for the estimation of turn-to-turn PDIV.

Several models are developed in the literature and can be separated into three categories: analytical equations, FEM (Finite Element Method) simulations, and probability models. Among them, several models are based on Paschen's law, which defines the breakdown voltage of a gas between two electrodes. Hence, first, Paschen's law is introduced and some notes on its use in twisted pair PDIV estimation are gathered.

2.2.1. Paschen's Law

Paschen's law describes the breakdown voltage for a given gas and electrode material under uniform electric field conditions, as a function of the product of gas pressure and gap length. This law is developed under constant pressure and temperature conditions [25]. The analytical expression derived for the breakdown voltage (V_B) is described in Equation (2):

$$V_B = B\frac{Pd_{air}}{ln\left(\frac{APd_{air}}{k}\right)} \tag{2}$$

$$k = ln\left(1+\frac{1}{\gamma}\right) \tag{3}$$

where A and B are experimental constants and depend on the gas composition (for air: 11.25 $Pa^{-1}m^{-1}$ and 273.75 $VPa^{-1}m^{-1}$, respectively, [58]), P is the air pressure, d_{air} is the path followed by the electronic avalanche (the electric field lines) , and γ is the Townsend's secondary electron emission coefficient, which describes the average released electrons from the cathode per incident positive ion [25]. It is important to note that this voltage is considered as peak to peak [59].

Despite Paschen's law being widely used in the literature for the estimation of the PDIV [38,53,59–68], its application to the case of enamelled twisted pairs presents some limitations that must be taken into account.

1. In the general use of Paschen's law (using parallel plate electrodes), for a given pressure, the first ionisation phenomena (α') is considered constant in the distance d_{air}, defining d_{air} as the perpendicular distance between electrode surfaces. Several authors have used the same definition to model the PDIV on twisted pairs with FEM simulations [60,68,69] or analytical models [59]. Indeed, the difference between the real and straight field length has been shown to be lower than 1% for small distances, while it is about 7% for distances larger than 50 µm [69]. Adversely, Gómez de la Calle et al. [70] stated that this simplification of assuming a constant effective first ionisation phenomenon is not correct for this specified geometry. In twisted pairs, the path defined by the perpendicular distance between wires does not match with the path followed by the electric field lines. Therefore, this approach is questioned.
2. Paschen's law is based on Townsend's ionisation mechanism. Although several authors used Paschen's law for the definition of the PDIV [59,60,62,63,70], in [70], the author notes that some works have proven that the streamer inception mechanism is more effective. Additionally, L. Lusuardi et al. [71] argued that, as enamelled twisted pairs, electrodes are covered by an insulation film, so the emission of secondary electrons from the insulated cathode by positive ions is extremely unlikely. Accordingly, Paschen's law can not be used to estimate the PDIV and should be replaced by the streamer criterion. The main concept of this criterion is the single-electron-avalanche mechanism, which defines the breakdown voltage of the air when the number of electrons reaches a critical number. The relationship between the number of electrons

along a field line and the critical electron number is defined by the Schumann criteria (Equation (4)):

$$k_s = \int_0^{d_{air}} \alpha_{eff}(x)\,dx = \ln N_c \quad (4)$$

where α_{eff} is the effective ionisation coefficient of the anode, N_c is the critical number of electrons for the breakdown, and k_s is a dimensionless constant, generally taken as 18 for air.

3. Independent of the use of Paschen's law or Schumann's criteria, there is no consensus in the literature regarding the definition of the value γ for Paschen's law and k_s for the Schumann criteria. Concerning γ, although it is well defined for metal electrodes, there is uncertainty about its value for different kinds of enamel materials [62,70]. Regarding the Schumann constant k_s, although it is generally defined as a constant value (18 for air), the prediction of the PDIV using this value seems not to be very accurate [71].
4. It is well known that the breakdown voltage of the air is affected by atmospheric conditions such as temperature, pressure, and humidity. Several authors [26,30,38,53,65,72] stated that Paschen's law is not valid for certain atmospheric conditions and proposed corrections for Equation (2).

Different kinds of solutions are proposed in the literature to overcome the issues related to the definition of Townsend's secondary ionisation coefficient (γ) and the Schumann's criteria constant (k_s), as well as to consider the influence of the temperature on the Paschen's law. These solutions are collected in the following lines.

Townsend's Secondary Ionisation Coefficient (γ) and Schumann's Criteria Constant (k_s) Correction

As mentioned before, researchers do not completely agree about the value of the γ coefficient. $\gamma = 0.01$ is a well-known value for metallic electrodes. Several researchers have obtained good accuracy in the estimation of PDIV by applying this value to polymeric enamelled twisted pairs [63,69]. On the other hand, others have adjusted the γ value in order to achieve good accuracy in the estimation of the PDIV compared to the experimental results. For instance, M. Szczepanski et al. [59] adjusted $\gamma = 0.001$, which best fits their experimental measurements using a PEI (Polyester-imide) and PAI enamel combination.

Bearing this in mind, P. Collin et al. [62] proposed a method to predict the γ value by iterations, based on a mixture of numerical and FEM calculations and comparing with the experimental results. Firstly, a FEM model is built by using a precise enamelled profile with the help of a microscope and representing the true experimental configuration. Then, the 2D electrostatic problem is solved using FEM, with the experimental PDIV value being the input of a high voltage conductor (see Section 2.2.3), to calculate the voltage drops along straight field lines between the wires. The computed voltage drops are compared to the Paschen's curve and the γ is iterated until the Paschen's curve intersects with the voltage drops. Using this method, $\gamma = 0.0006$ is proposed by [62] for PAI overcoat samples. Moreover, negligible differences are observed for different diameters, meaning the same γ value can be used.

A similar methodology was proposed by M.Gomez de la Calle et al. [70] but by considering constant electric field lines to define d_{air}. In this case, the γ value is defined as 0.0078 based on the arithmetic mean of the value estimated for different diameters and relative permittivity values (the materials have different epoxy resins, not specified). It is shown that using this mean value, the maximum error achieved in the estimation of PDIV for different wire diameters and permittivity values at room temperature is about 5%. The same process for the estimation of γ is developed at 100 and 150 °C, showing that γ tends to decrease with an increase in the temperature. Nonetheless, after analysing the errors and variations in the estimation, the author concludes that the changes in the material type and manufacturer are more important than those in the temperature.

Finally, Y. Kemari et al. [73] proposed a different method for γ estimation. In a similar way to [70], the electric field lines and scalar potential were computed using FEM. Then, the results were integrated into self-developed software to predict the PDIV using Townsend's theory in a range of γ from 10^{-6} to 10^{-2}. The γ was interpolated for the defined experimentally PDIV. This way, $\gamma = 0.00065$ was proposed for the PI (Poly-imide). In this case, the dependency on the temperature was also studied, showing an increasing tendency, contrary to [70], but with a negligible variation. Moreover, using γ approximated at 20 °C for temperatures up to 200 °C to predict the PDIV did not lead to an appreciable difference, which is in agreement with [70].

Concerning the Schumann criteria constant (k_s), as mentioned before, it is generally established at 18 for air. However, L. Lusuardi et al. [71] showed that this value must be adjusted depending on the specific electric field. Indeed, they proposeed an iterative method to define this value. Firstly, a FEM analysis was carried out in a similar way to [70], defining the measured PDIV as the input voltage to determine the electric field across each field line in the air wedge between the wires. Then, they imported gas ionisation parameters as a function of the specific electric field. Finally, the integral described in Equation (4) was evaluated. Starting with $k_s = 18$, if $k_s \geq \int_0^{d_{air}} \alpha_{eff}(x)\, dx$ for at least one electric field line, k_s is defined. Otherwise, k_s is reduced and the last step repeated. Using this process, $k_s = 5.98$ was defined from the mean value of the different wire diameters and enamel permittivity, with a maximum error of 9% for room and high temperatures.

Temperature Correction

Two main corrections were applied to Paschen's Equation (2) in order to consider the influence of the temperature. On the one hand, the Peek correction was based on the gas density, considering the ideal gases law with constant volume. The air density was adjusted from reference conditions to new pressure and the temperature as in Equation (5). The expression described by Paschen's law (Equation (2)) was corrected as in Equation (6) [65,72]:

$$\rho = \frac{P_{new}}{P_{ref}} \frac{T_{ref}}{T_{new}} \tag{5}$$

$$V_B(P_{new}, T_{new}) = \rho V_B(P_{ref}, T_{ref}) \tag{6}$$

On the other hand, the Dunbar correction, based on the Gay–Lussac law, consists of obtaining an equivalent pressure considering the surrounding air as a perfect gas (Equation (7)). Then, Paschen's Equation (Equation (2)) is solved with this equivalent pressure [65,70–72]:

$$P_{equivalent} = P_{ref} \frac{T_{ref}}{T_{new}} \tag{7}$$

According to [65,72], the Dunbar correction correlates better to their results than the Peek correction at atmospheric pressure. Nonetheless, for Sili et al. [65], when the temperature and pressure were combined, both corrections no longer followed the behaviour of the experimental points. In the manner of [70,71], good results were achieved using the Dunbar correction.

2.2.2. Analytical Equations

It is necessary to take into account the fact that some assumptions and simplifications might be used to estimate the PDIV. Due to these simplifications, analytical models generally are less precise than the FEM simulations. The main advantage is that a much lower computational load is required.

Dakin Model

Dakin et al. [74] measured the PDIV value on a wide range of insulating materials and thicknesses and presented an empirical equation, Equation (8), based on the relationship between the insulation thickness and its relative permittivity:

$$\text{PDIV} = 163\left(\frac{t_{\text{ins}}}{\varepsilon_{\text{r}}}\right)^{0.46} \tag{8}$$

where the PDIV is provided in V_{rms}, t_{ins} is the total insulation thickness in μm , and ε_r is the relative permittivity of the insulation. In the twisted pairs, t_{ins} is twice the enamel thickness (as there is one layer in each conductor) and, in the case of using different enamel materials, the mean value of the relative permittivity should be used ($\bar{\varepsilon_r}$).

Despite this equation fulfilling a wide range of insulation thicknesses and relative permittivity values, the environmental conditions of the measurements, such as temperature, are not considered.

Parallel-Plate Capacitor Model

M. Szczepanski [59] proposed a PDIV prediction model for twisted pairs based on two well-known equations. On the one hand, it simplifies a twisted pair as a parallel-plane capacitor with two copper conductors separated by an enamel–air–enamel layer. It assumes that the thickness of the enamel (in μm) is significantly lower than the diameter of the copper wire (in mm), so its curvature can be neglected. Therefore, the series capacitor simplified insulation model from Equation (9) proposed by [75] can be used. On the other hand, bearing in mind that the PDIV is the minimum voltage at which the voltage across the air gap is equal to the breakdown voltage of the air, defined using Paschen's law [25] (Equation (2)), it concludes that the PDIV is the lowest total voltage V, where $V_{air} = V_B$ for different air gap sizes (Equation (10)).

$$V = \left(\frac{V_{\text{air}}}{d_{\text{air}}}\right)\left(d_{\text{air}} + \frac{t_{\text{ins1}}}{\varepsilon_{\text{r1}}} + \frac{t_{\text{ins2}}}{\varepsilon_{\text{r2}}} + \dots\right) \tag{9}$$

$$\text{PDIV} = min\left[\left(\frac{V_{\text{B}}}{d_{\text{air}}}\right)\left(d_{\text{air}} + \frac{t_{\text{ins1}}}{\varepsilon_{\text{r1}}} + \frac{t_{\text{ins2}}}{\varepsilon_{\text{r2}}} + \dots\right)\right] \tag{10}$$

where V is the voltage between conductors, V_{air} is the voltage in the air gap, d_{air} is the thickness of the air gap, V_B is the air breakdown voltage defined by Equation (2), and t_{insi} and ε_{ri} are the thickness and the relative permittivity of each insulation layer, respectively.

As Paschen's law is used to develop Equation (10), the limitations described in Section 2.2.1 are directly derived in this model. Firstly, as mentioned, the author assumes that the twisted wire can be simplified to a parallel plane capacitor neglecting the curvature of the enamel and, thus, the air gap distance is defined as the straight distance between electrodes. Secondly, Townsend's criteria are used, with difficulties adjusting the γ (as mentioned by the authors). Finally, the temperature dependence of the Paschen's curve is not considered.

Lusuardi Model

Based on the experimental results from measuring the PDIV at different pressure levels using 50 Hz AC, L. Lusuardi et al. [26] proposed an analytical model for the estimation of the PDIV at different pressure and temperature levels. First, they defined a new empirical model using linear regression based on the PDIV measured values as a function of the logarithm of pressure (in bar). Then, since the ionisation process depends on the mean free path, which is inversely proportional to the number density (number of gas molecules per cubic meter), they reported the results as a function of the number density. The number density is dependent on the pressure and temperature, so Equation (11) can be deduced as normalised to reference values.

$$\frac{\text{PDIV}_{P_{\text{new}},T_{\text{new}}}}{\text{PDIV}_{\text{ref}}} = 1 + 0.299\ln\left(\frac{P_{\text{new}}}{P_{\text{ref}}}\frac{T_{\text{ref}}}{T_{\text{new}}}\right) + 0.0446\ln\left(\frac{P_{\text{new}}}{P_{\text{ref}}}\frac{T_{\text{ref}}}{T_{\text{new}}}\right)^2 \tag{11}$$

where $\text{PDIV}_{P_{new},T_{new}}$ is the estimated PDIV value at the desired pressure and temperature, PDIV_{ref} is the experimentally measured PDIV value at the reference pressure and

temperature, P_{ref} and T_{ref} are the pressure and temperature at which experimental PDIV measurement is collected, respectively, and P_{new} and T_{new} are the pressure and temperature at which the PDIV is estimated, respectively.

The author's reasoning for the use of this model is that the Paschen's curve is not able to adequately reproduce the dependency of the measured PDIV on pressure. However, the author mentions that it is not valid if the relative permittivity has a considerable dependency on the temperature. The maximum temperature analysed is far from the glass transition temperature and the permittivity change is negligible within this temperature range for the used samples. Hence, this model might not be valid for insulations with glass transition temperatures close to the operating temperature. In this kind of insulation, the contribution of the permittivity increases at high temperatures, so the permittivity should be considered as a separate variable.

Estimation Considering Rise Time and Pulse Width

Based on the extended volume–time theory, explained later, Wei et al. [43] proposed a model to estimate the PDIV for a single pulse based on the experimental results, where the rise time and pulse width are considered. Assuming that the initial electron generation probability (defined using the Extended Volume–Time theory) can be approximated as the accumulated PD probability, the authors stated that this probability can be obtained from the experimental PDIV value and time delay value (the time period since the applied voltage meets the ignition voltage until the PD is developed; see Figure 5).

$$P(t) = 1 - e^{-A(t-t_0)} \tag{12}$$

$$P(t) = 1 - e^{-A\left(t - \frac{V_{inc} t_r}{0.8 V_{apply}}\right)} \tag{13}$$

where A is the equivalent initial electrons from the air volume and enamel layer surface and t_0 is the time when the ionisation process starts. Under the same environmental conditions, t_0 corresponds to the instant at which the applied voltage (V_{apply}) is equal to the inception voltage (V_{inc}). In this case, the authors considered that the ignition voltage is the measured PDIV in the test sample under a constant DC voltage. As the rise time (t_r) is defined between 10% and 90% of the applied voltage, a 0.8 factor is used. Therefore, Equation (12) can be rewritten as Equation (13).

With the aim of simplifying the acquisition of the equivalent initial electrons, the authors propose Equation (14) for the quantification of A, considering Equation (13) and experimental PDIV (defined when the probability is 50%) and delay time data.

$$A(V_{apply}, t_r) = a {V_{apply}}^b c {t_r}^d \tag{14}$$

where $a = 1.038 \times 10^{-4}$, $b = 7.542$, $c = 211.4$, and $d = -1.149$ with a goodness R^2 fitting of 0.9409 based on 100 ns data. V_{apply} and t_r are in kV and ns, respectively. The term $(c {t_r}^d)$ is a correction function that equals 1 when the rise time is 100 ns. In order to introduce the impact of the pulse width, the authors conclude that the critical number of electrons necessary to trigger the PD is relatively stable regardless of the pulse width and rise time. Hence, the number of critical initial electrons generated can be described by the Equation (15). The term $(V_{inc} t_r / 0.8 V_{apply})$ is negligible compared to the pulse width (in µs). Thus, based on Equations (14) and (15), the relationship between PDIV, pulse width t_w (in µs) and rise time t_r (in ns) can be defined as in Equation (16):

$$N_o(t_w) = A\left(t_w - \frac{V_{inc} t_r}{0.8 V_{apply}}\right) \tag{15}$$

$$\text{PDIV} = \left(\frac{N_o(t_w)}{ac}\right)^{\frac{1}{b}} {t_w}^{-\frac{1}{b}} {t_r}^{-\frac{d}{b}} \tag{16}$$

Intending to simplify the model, the authors also propose an alternative considering a reference value (Equation (17)), being $n = -0.1142$ and $m = 0.01818$ with a goodness R^2 fitting 0.9484.

$$\text{PDIV} = \text{PDIV}_{t_w=100\,\mu s, t_r=120\,ns} \left(\frac{t_w}{100}\right)^n \left(\frac{t_r}{120}\right)^m \quad (17)$$

This model is suitable only for cases in which there is neither an overvoltage in the applied voltage waveforms nor space charge accumulations. Indeed, the authors mention that the space charge distribution can be different depending on the rise time, due to the fact that the rise time can impact the electron generation rate. Moreover, as the model is developed for a specific insulation enamel material at room temperature, the constant values (a, b, c, and d) would possibly not fit other insulation enamels and temperatures, so new experiments would be necessary to adjust the model. The temperature will most likely change the A values, as V_{inc} would be reduced with the increase in temperature. Nonetheless, the main benefit of this model is that it offers a good approximation for the estimation of PDIV in a relatively simple way, considering rise time and pulse width at ambient temperature for a specific enamel.

2.2.3. FEM Simulations

Two different approximations have been identified in the literature for the estimation of the PDIV based on the FEM simulations. In all of them, the FEM simulations are developed in order to determine the electric field or potential difference across two insulated wires [38,60,62,63,69,70]. The geometry used is defined as in Figure 6. Then, the results are evaluated by applying different methods to define the PDIV value (Paschen's law or Schumann criteria).

The FEM model attempts to simulate the most critical situation of turn-to-turn insulation, where one conductor is subjected to high voltage (HV, defined as peak-to-peak voltage) and the other to 0 V (GND) and there is no impregnation. d_{in} is the conductor nominal diameter, t_{ins} is the insulation thickness, d_0 is the minimum distance between wires, d is the horizontal distance between the wires, and d_e is the length of the electric field line. Using this model, the voltage distribution of the air gap is computed in the range of the gap distance (defined as d or d_e).

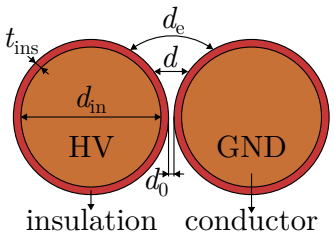

Figure 6. FEM model geometry.

FEM and Paschen's Law

In order to define the PDIV value using a combination of FEM and Paschen's law, FEM simulations for different voltage level inputs are developed. The voltage distribution of the air gap in the range of gap distance is calculated using FEM and subsequently compared to Paschen's law (Figure 7). If the FEM curve crosses the Paschen's curve, there is PD activity. If the FEM curve does not cross the Paschen's curve, there is no PD activity. Thus, the PDIV is defined as the point where the FEM curve is tangential to the Paschen's curve, as shown in Figure 7.

The main idea behind this method is included by different authors. Nevertheless, as described in Section 2.2.1, there is no agreement in the literature as to whether d_{air} is defined as the horizontal distance between the wire surfaces (defined as d in Figure 6) or the path followed by the electric field lines must be used (defined as d_e in Figure 6) to define the distance followed by the electrons (d_{air} in Equation (2)).

The straight-line distance between the two surfaces is used to define the electric field in [38,60,62,69]. Indeed, when using a straight distance, an error of around 2% [69], less than 5% [60], and less than 3% [38] is reported in the literature in the estimation of the PDIV. Additionally, of the cited studies, [38] obtained PDIV values for different temperatures by considering the permittivity dependence on the temperature and the Paschen's curve temperature correction. In the case of [62], this method was used to obtain the γ value as described in Section 2.2.1.

However, other authors [63,70] used constant electric field lines to estimate the PDIV and defined the γ value based on the reasons stated in Section 2.2.1. For that, the electric field in the air gap between the wire surfaces is first computed using FEM. Then, constant electric field value points are identified and a function based on a second-order polynomial is defined. Finally, the d_e is calculated using the integral of polynomial between two points.

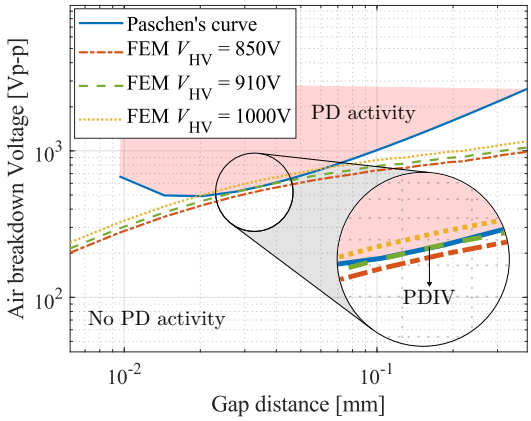

Figure 7. Schematic description of PDIV definition using FEM and Paschen's law.

FEM and Schumann Criteria

As explained in Section 2.2.1, L. Lusuardi et al. [71] reported that, in twisted pairs, there are nonuniform electric fields. Moreover, the emission of secondary electrons from the insulated cathode is unlikely, so Paschen's law cannot be used to predict the PDIV and must be replaced by the streamer inception criterion. With this criterion, the PDIV is defined as when the number of electrons of an electric field line fulfils the Schumann criteria.

The method proposed by L. Lusuardi et al. [71] uses FEM simulation and Schumann criteria to define the PDIV, considering the effect of the temperature. The Schumann constant is defined as 5.98, as explained in Section 2.2.1. The method consists of the following steps:

1. Define an initial voltage for the 2D FEM simulation model and compute the electric field and the constant electric field line length, similar to in [70].
2. Import a database of gas ionisation parameters as a function of the specific electric field $\alpha_{\text{eff}}(E/P_{\text{equivalent}})$. Where $P_{\text{equivalent}}$ is defined as in Equation (7).
3. Verify if the Schumann criteria are satisfied (4) for at least one electric field line. If not, repeat the process, increasing the voltage.

With the proposed method, the author obtains the maximum error of 9% between the experimental and model data for different wire diameters at 25 and 150 °C. M. Gomez de la Calle [76] exposes the comparison between the use of Paschen's law and Schumann's criteria for the definition of the PDIV using a combination of each criterion with FEM simulations, as defined in [70] and [71], respectively. At room temperature, Paschen's law is chosen, since the prediction error is reduced from 4.19% using Schumann's to 2.36% using Paschen's. However, the difference between the methods is reduced at 150 °C, where a 7.16% and 7.05% error is reported for Schumann's and Paschen's, respectively. Moreover, if the PDIV for humid environments (not considered in both models) is desired, the estimation error increases to 15%. Thus, it is concluded that using one model instead of the other is

not so relevant, as long as external uncertainties, not considered in the models, have greater error values.

2.2.4. Probability Model

Both analytical and FEM-based models refer to a deterministic approach and, when certain conditions are met, PD will occur. However, this assumption is not always fulfilled. As mentioned several times in Section 2.1, the time when the applied voltage is maintained above the ignition is a key factor in the initial electrons' availability. If the applied voltage is maintained during too short a period, for example in overshoots, even though the applied voltage is higher than ignition, it is unlikely that initial electrons will be available. Therefore, probabilistic PDIV estimation models combining the probability associated with the initial electron availability and the inception voltage condition are developed considering the applied voltage evolution over time. Within these models, the volume–time theory deals with the air gap initial electrons' generation probability in consideration of temporal and spatial change in electric field distribution, to estimate discharge inception at bare electrodes. Based on this theory, N. Hayakawa et al. [31] proposed the extended volume–time theory, where, in addition to the number of electrons detached in the air gap, it also considers the number of electrons generated using electronic emission from the enamel coating of electrodes. The probability of initial electrons can be computed as described in Equation (18) and the PDIV is defined as when this probability is 50%.

$$P(t) = 1 - e^{\int (R_V(t) + R_S(t))\mathrm{d}t} \tag{18}$$

$$R_V(t) = \int_{V_{cr}} r_V \left(1 - \frac{\eta}{\alpha}\right) \mathrm{d}V \tag{19}$$

$$R_S(t) = \int_{S_{cr}} r_S \left(1 - \frac{\eta}{\alpha}\right) \mathrm{d}S \tag{20}$$

where $R_V(t)$ (Equation (19)) is the air gap initial electrons and $R_S(t)$ (Equation(20)) represents the initial electrons on the enamel surface. V_{cr} and S_{cr} stand for the critical air gap volume and enamel surface, respectively. r_V and r_S are the initial electron generation rates per unit time for the unit volume and unit surface. α is the electron impact ionisation coefficient and η the electron attachment coefficient.

On the one hand, V_{cr} and S_{cr} are calculated using electric field analysis using FEM, where Schumann's Equation (Equation (4)) should be satisfied. Accordingly, V_{cr} is defined as the volume comprising the air gap points where, for the specific electric field, the Schumann criteria is met. Similarly, S_{cr} is defined for the enamel surface points. The authors do not specify the definition of the Schumann criteria constant, which is a key factor, as explained in Section 2.2.1. The critical surface and volume increase with the enhancement of the electric field. r_V and r_S depend on the instantaneous electric field strength, as defined in Equations (21) and (22), respectively.

$$r_V = k_d n^- \tag{21}$$

$$r_S = aE^2 e^{-\frac{b}{E}} \tag{22}$$

where n^- is the O_2^- density, a constant irrespective of time and space, and k_d is the expected electron impact ionisation frequency, which depends on electric field strength. a and b are experimentally provided based on the Fowler–Nordheim Equation [77]. As shown by the author of [31], r_V tends to stabilise with an increase in the electric field, whereas r_S sharply increases even at high electric fields, which can generate initial electrons in the air gap with enamel-coated electrodes.

Several observations were recorded by the authors in [31]. First, both $R_V(t)$ and $R_S(t)$ increased with the applied voltage. This behaviour was also noted in [43] based on the experimental results. On the other hand, the authors concluded that $R_S(t)$ can be more useful for PDIV estimation, as it has a higher increase rate and a higher value. That means

that the initial electrons would mainly originate on the enamel coating rather than in the air gap. Secondly, the PDIV decreased with an increase in the sum of provided initial electrons independent of the applied voltage waveform. The higher the sum of the provided initial electrons, the higher the probability of ignition. Finally, with the use of the probabilistic model, the PDIV can be estimated for different waveform characteristics, independent of having to overshoot or not.

Using this model for PDIV estimation provides the opportunity to calculate the PDIV in the case of overshoot or fast rise time and narrow pulse width waveforms. Consequently, it can be a key point for the PDIV estimation of turn-to-turn insulation feed using WBG. However, the authors do not analyse how the model behaves in different environmental conditions, for example, at different temperatures.

2.2.5. Summary of PDIV Estimation Models

The most relevant matters of the models analysed in this section are summarized in Table 2. For each model, the data used, changing ambient and electrical variables considered, pros and cons, and studies where the models are used are collected.

Table 2. Summary of PDIV estimation models.

Model	Use Data	Changing Variables					Pros	Cons	Ref.
		T	***P***	***HR***	t_r	t_w			
Dakin	ε_r, t_{ins}	✓ *	x	x	x	x	Simple and ↓ computational cost. Independent on insulation enamel material and diameter	Room conditions	[38,59,74,78]
Parallel plate	ε_r, t_{ins}, A, B, γ, d_{air}	x	✓	x	x	x	Simple and ↓ computational cost. Independent on insulation enamel material and diameter	Room conditions. Difficult to define γ	[59]
Lusuardi	T_{ref}, P_{ref}, $PDIV_{ref}$	✓ **	✓	x	x	x	Simple and ↓ computational cost	Not valid for high ε_r change with T. Neccesary experimental PDIV	[26]
Considering t_r and t_w	ε_r, t_{ins}, $PDIV_{ref}$	x	x	x	✓	✓	Simple and not high computational cost	Room conditions and possibly necessary adjustment with experiments	[43]
FEM and Paschen's straight distance	ε_r, t_{ins}, A, B, γ, d_{air}	✓	✓	x	x	x	Independent on insulation enamel material and diameter	↑ computational cost. Difficult to define γ	[38,60,62,69]
FEM and Paschen's cte. E field lines	ε_r, t_{ins}, A, B, γ, d_{air}	✓	✓	x	x	x	Independent on insulation enamel material and diameter	↑↑ computational cost. Difficult to define γ	[70]
FEM and Schumann cte. E field lines	ε_r, t_{ins}, α_{eff}, k_s, d_{air}	✓	✓	x	x	x	Independent on insulation enamel material and diameter	↑↑ computational cost. Difficult to obtain air property database and define k_s	[71]
Extended volume–time theory	ε_r, t_{ins}, d_{air}, $R_V(t)$, $R_S(t)$	x	x	x	✓	✓	Independent on insulation enamel material and diameter. Temperature and pressure correction can be implemented	↑↑ computational cost, FEM used.	[31,43,61]

✓considered. x not considered. * Only consider change in ε_r. ** Only consider change in air properties. ε_r: relative permittivity; t_{ins}: insulation thickness; A: experimental constant for Paschen's curve (for air 11.25 $Pa^{-1}m^{-1}$) , B: experimental constant for Paschen's curve (for air 11.25273.75 $VPa^{-1}m^{-1}$), γ: Townsend's secondary electron emission coefficient, d_{air}: path followed by the electronic avalanche, T_{ref}: temperature for a reference PDIV measurement, P_{ref}: pressure for a reference PDIV measurement, $PDIV_{ref}$: reference PDIV measurement, α_{eff}: effective ionisation coefficient of the anode, k_s: Schumann criteria constant, $R_V(t)$: air gap volume initial electrons, and $R_S(t)$: enamel surface initial electrons.

3. Materials and Methods

The experiments are developed to analyse and contrast the performance of several PDIV modelling techniques from the literature at different temperatures. In this section, the samples, set up, and PDIV definition procedures employed to obtain our own experimental results are explained.

3.1. Samples

Twisted pair samples are widely used in order to reproduce the most demanding conditions of turn-to-turn insulation, where the first and last turn of the coil can be adjacent to each other [26,33,61]. For the experiments developed, Grade 2 enamel circular wires complying with UNE-EN-IEC 60317-0-1 [79] were used to prepare twisted pairs as specified in IEC 60172 [80].

Three different enamel wires were prepared for the experiments; their specifications are summarised in Table 3. Figure 8 illustrates the evolution of the relative permittivity of each sample group for different temperatures at 1 kHz provided by the manufacturer.

Table 3. Sample specifications.

Group Name	Wire Copper Diameter (mm)	Insulation Base Coat	Base Coat Percentage (%)	Insulation Surface Coat	Surface Coat Percentage (%)	Thermal Class (°C)
B	0.8	Polyester (PE)	72	PAI	28	200
C	0.9	-	-	PI	100	240

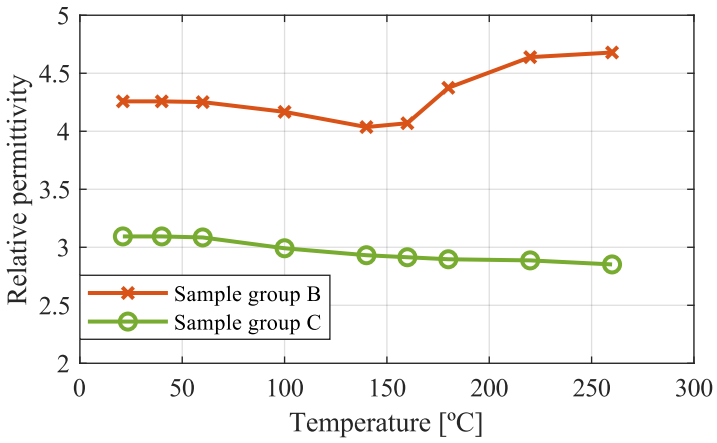

Figure 8. Permittivity evolution of the temperature measured at 1 kHz. Provided by the manufacturer.

3.2. Set Up

Figure 9 a represents the set-up for the PDIV measurement. It consisted of LT400W commercial PDIV measurement equipment from EDC (Electrical Dynamic Company , Milan, Italy) (UNE-EN 60270 [81]). One side of the sample was connected to the high-voltage (HV) lead of the equipment and the other to the grounded lead (GND). The sample was placed in an industrial oven with temperature control (Nabertherm 30–3000 °C) (Figure 9b). Before proceeding with the measurement, the sample was conditioned for 10 min after the desired temperature was reached. The samples were stored in a laboratory with an air conditioning system at room temperature conditions before the PDIV measurements. The relative humidity range in this type of room is 45–60% according to [82].

(a) (b)

Figure 9. Experimental set-up for PDIV measurement at different temperatures: (**a**) schematic; (**b**) real layout.

3.3. PDIV Measurement Procedure

To define the PDIV, the 50 Hz sinusoidal voltage was increased by 10 V/s from 0 until the first PD was detected. The minimum PD charge to be considered as PD was defined at 0.05 nC. As specified in UNE-EN 60270:2002 [81], this value should be defined as at least twice the background noise in pC before the measurements; 0.05 nC showed good agreement between surrounding noise avoidance and PD detection for all the developed experiments. Therefore, the first voltage level at which a PD with a charge equal to or higher than 0.05 nC occurs was defined as the PDIV. For each condition, the average of five freshly manufactured sample data points were used to define the PDIV value [24,36,83]. Each sample was measured three times with an interval of 60 s between measurements, in order to avoid the memory effect [41,43], and the average value is used. The results are represented by the average, maximum, and minimum measurement values.

4. Analysis of PDIV and Modelling Tool Performance for Variable Temperature

From the literature review (see Section 2), it was clear that the temperature affects the PDIV. Considering that an electric machine's winding can reach up to 180 °C during operation [84], it is of major importance to regard high temperatures during the design. This section studies the effect of the temperature on the PDIV and the performance of several PDIV modelling tools at high temperature.

4.1. The Effect of Temperature on PDIV

As mentioned in the literature review, the temperature largely affects the air properties and enamel permittivity. To distinguish between the effects of the two factors, two models (explained in Section 2.2), which consider air properties or relative permittivity to estimate the PDIV, were used. The first model, Dakin model, proposed in [74], can consider the change of the relative permittivity. The second model, Lusuardi model, proposed in [26], takes into account the effect of the air density on the evolution of the PDIV. In the analysis, room temperature PDIV measurements of sample group C (624.5 Vrms) and sample group B (627.2 Vrms) were collected as a reference, where the permittivity was more stable with the temperature (variation: 7%) or varied by 16%, respectively, (Figure 8).

Figure 10 shows the comparison between the effect of the relative permittivity (using the Dakin model presented in [74]) and the air density (using the Lusuardi model proposed in [26]) on the PDIV with the increase in temperature. In Figure 10a, the difference in the air density and both materials' permittivity with the temperature is depicted. The evolution is normalised for each variable value at room temperature. It is clear that the air density is the major factor affected by temperature. Accordingly, it is expected that the PDIV evolution is more affected by the Lusuardi model [26] than by the Dakin model [74]. This is clear in Figure 10b. The PDIV is more affected due to the air density than the

permittivity. It can be concluded that the predominant factor affecting the PDIV due to the temperature is the change in air properties. Consequently, even if the relative permittivity of the insulation material is reduced with the temperature, the combined effect will generally tend to decrease the PDIV with temperature. This is reinforced by the experimental results shown later in Sections 4.2.1 and 4.2.2.

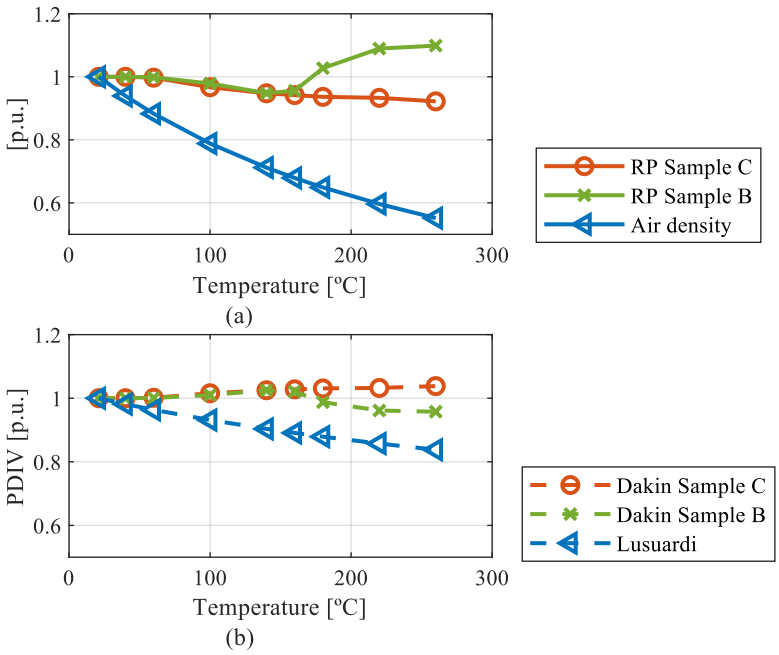

Figure 10. Comparison of the effect of temperature: (**a**) proportional evolution of air density and relative permittivity; (**b**) proportional evolution of the PDIV based on the Dakin and Lusuardi models (Relative Permittivity (RP)).

All in all, the PDIV is affected by temperature due to the decrease in air electric breakdown strength and the dependence of relative permittivity on temperature. Despite the temperature decreasing the relative permittivity for some enamel materials (sample group C, for example), which can increase the PDIV, the effect of temperature on the air density is more significant to define. It can be said that, generally, a temperature increase has the inverse effect on the PDIV. For instance, at 180 °C, the relative permittivity of sample C ($\varepsilon_r = 2.89$ at 180 °C) should decrease by around 25% in order to neutralise the effect of the air. Nonetheless, the air properties and relative permittivity should be considered to evaluate in what proportion the PDIV decreased with temperature.

4.2. Performance of PDIV Models for Variable Temperature

4.2.1. Dakin Model

The Dakin model was proposed in [74] and defined as Equation (8) (see Section 2.2). In spite of the relative permittivity being adjusted to the specified temperature, the dependency of the breakdown voltage on the temperature is neglected, which can result in a less accurate PDIV estimation at high temperatures.

In Figure 11, the comparison between the PDIV values estimated using the Dakin model (considering the evolution of the relative permittivity with temperature) and the experimental PDIV measurements for sample group B at different temperatures is illustrated. It is shown that the PDIV calculated using the Dakin can fit the experimental value at temperatures below 60 °C with a maximum error of around 10%. Above this temperature, the error keeps increasing with the increase in the temperature and can produce values up to around 27% at 180 °C.

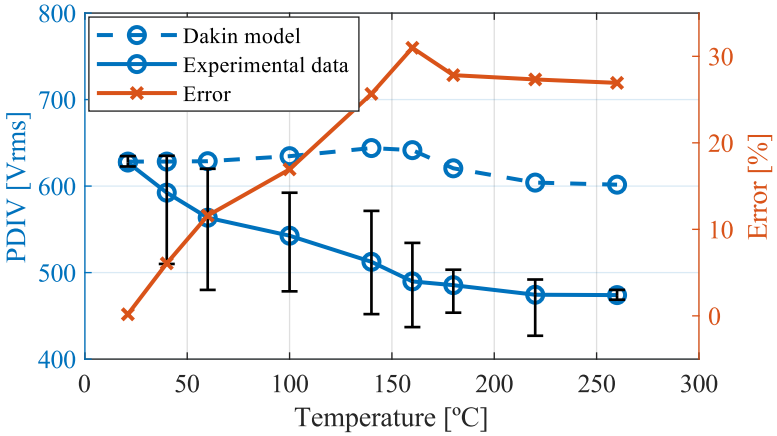

Figure 11. Comparison of experimental measurements and Dakin PDIV estimation for different temperatures (sample group B).

It could be concluded that only considering the evolution of permittivity with temperature is not enough to accurately predict the PDIV. The effect of the temperature on air properties must be considered, especially at high temperatures. Thus, the Dakin model is not suitable for PDIV estimation during operating conditions for electric motors, where the winding temperature can reach 180 °C. Even so, the Dakin model was widely used in the literature [38,59,78] due to its accuracy and simplicity at ambient temperature.

4.2.2. Parallel-Plate Capacitor Model

Parallel-plate model as described in [59] was used (see Equation (9), Section 2.2). Figure 12 shows the comparison between the experimental results (sample group C) and the use of the parallel-plate model for different temperatures. The permittivity of the corresponding temperature and $\gamma = 0.001$ were used.

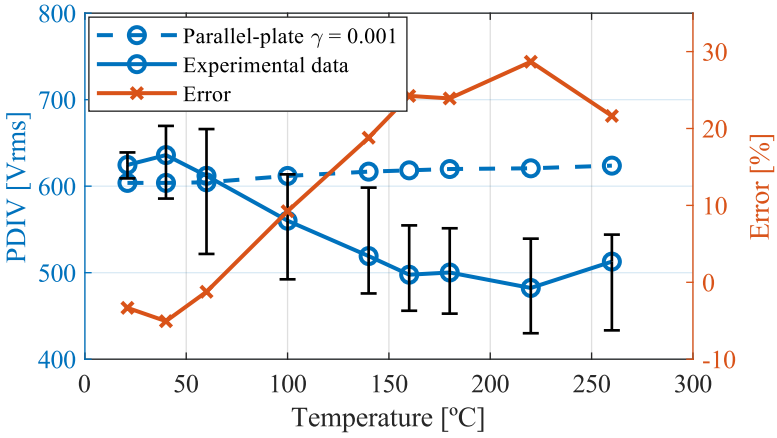

Figure 12. Comparison of experimental measurements and parallel-plate model (sample group C).

On the one hand, it can be seen in Figure 12 that the use of $\gamma = 0.001$ results in an error of around 5% at room temperature. On the other hand, at higher temperatures, the error is increased by around 25%. Similar to the Dakin model, the parallel-plate model can provide accurate results at low temperatures. However, not considering the air properties results in a considerable error at temperatures higher than 140 °C. Therefore, this model could not be used to accurately estimate the PDIV at operating conditions of an electric motor.

4.2.3. Lusuardi Model

In contrast to the Dakin and parallel-plate models, the Lusuardi model considers the effect of the temperature on the surrounding air properties. The Lusuardi model was

proposed in [26] and defined as Equation (11). In Figure 13, the experimental results compared to the Lusuardi model for sample groups B (greater change of permittivity with temperature) and C (lower change of permittivity with temperature) are illustrated.

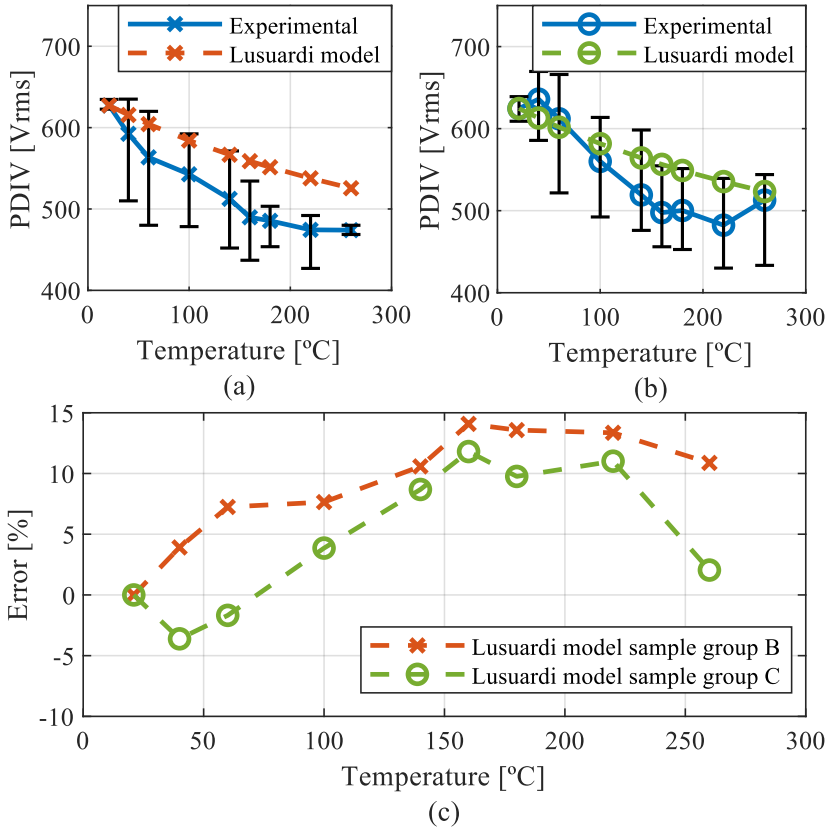

Figure 13. Comparison of experimental measurements and Lusuardi model: (**a**) sample group B (higher dependence of the permittivity on temperature); (**b**) sample group C (lower dependence of the permittivity on temperature); and (**c**) error of the model.

It can be seen in Figure 13 that the model best fits to sample group C, whose permittivity is less dependent on the temperature. In this case, the model results remain inside the uncertainty range of the measurement, with a maximum error of around 10%. Adversely, due to the higher influence of the permittivity on sample group B, the calculated values for the PDIV at high temperatures are outside of the measurement uncertainty. However, the accuracy could be considered acceptable as the maximum error is around 12%. As the author of [26] mentions, the difference between the obtained results for both sample groups may be attributed to the influence of the relative permittivity. Therefore, the estimation error is higher when the permittivity variation with the temperature is increased.

The main drawbacks of the Lusuardi model are the requirement of an experimental PDIV value and the non-consideration of the relative permittivity. All in all, this model could accurately estimate the PDIV at operating temperatures.

4.2.4. FEM and Paschen's Law

The combination of FEM and Paschen's law was widely used in the literature to estimate the PDIV [38,60,62,63,69,70]. However, there was no consensus on the definition of d_{air} in Paschen's law (Equation (2)) for twisted pairs. Therefore, the use of both d_{air} definition methods identified in the literature (see Section 2.2) was evaluated. When considering the straight line, the model was defined as in [38,60,62,69]. In the case of the constant electric field, the lines were considered and the model was defined as in [70].

The experimental and model results for different temperatures are depicted in Figure 14. Sample groups B and C were used and the specifications for the models are defined in

Table 4. t_{ins} was defined as the minimum insulation thickness according to IEC 60317-0-1 [85]. The selected d_0 value was widely used in several studies [38,60,69]. Finally, γ for group B was defined as the value that best fitted the experimental room temperature results, based on the method explained in [62]. For group C, the value proposed in [73] was selected. In all cases, the permittivity dependency on the temperature and Dunbar Paschen's law corrections were applied as defined in [38,70].

Table 4. FEM and Paschen's law model specifications.

Group Name	d_{in} (mm)	t_{ins} (mm)	d_0 (mm)	γ
B	0.8	0.28	0.001	0.0002
C	0.9	0.2975	0.001	0.00065

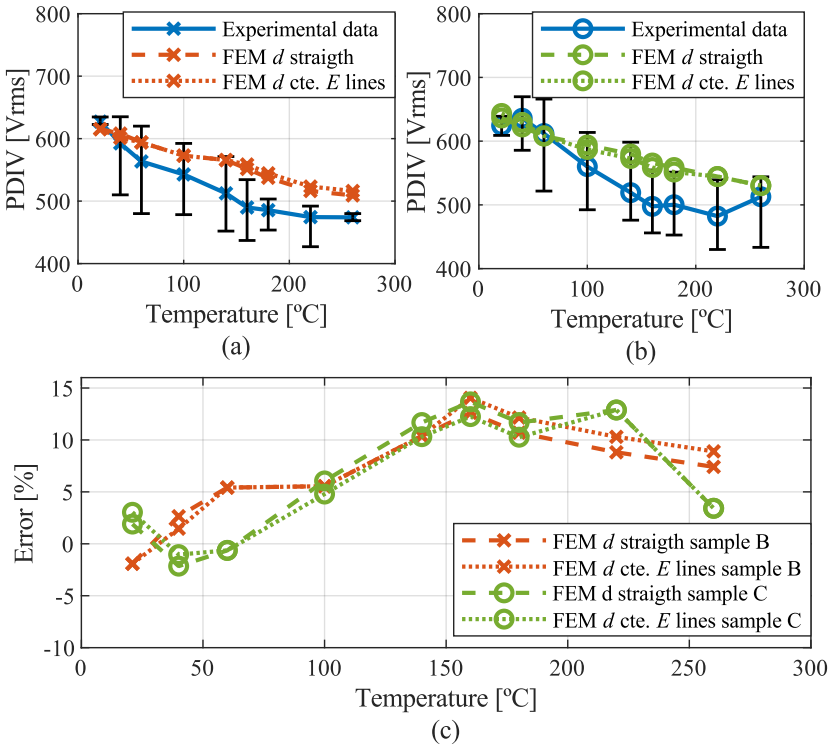

Figure 14. Comparison of experimental measurements and FEM and Paschen's law models: (**a**) sample group B; (**b**) sample group C; and (**c**) error of the model.

As observed in Figure 14, the results for the PDIV estimation using straight lines or constant electric field lines do not vary from each other. Indeed, as mentioned by [69], the difference between the length of the straight lines and constant electric field lines is not higher than 1%. With both methods, the maximum error for the analysed range of temperature is lower than 15%. In the case of sample group C, the estimation is into the uncertainty limits of the measurements, whereas the estimation for sample group B is not. This difference could be due to the effect of moisture (not considered in the models) or the uncertainty in sample thickness and geometry due to temperature [73]. Based on the lack of difference in the PDIV estimation, considering the straight distance between conductors might be more convenient for twisted pairs. The computational load necessary to develop constant electric field lines analysis in comparison with straight lines is higher.

Overall, the FEM and Paschen's law model can provide accurate results for the estimation of the PDIV at high temperatures. Additionally, the model takes into account the changes in permittivity. Nevertheless, it requires a high computational load, especially if constant electric field lines are used.

4.2.5. Proposed Model

Within the previously analysed models (Dakin, parallel-plate, Lusuardi, and FEM and Paschen's law), Lusuardi and FEM and Paschen's law models were the ones capable to obtain good accuracy on the estimation of the PDIV at high temperatures. However, the Lusuardi model needed an experimentally measured PDIV value and did not consider the insulation permittivity, while the FEM and Paschen's law model required a high computational load. Hence, in order to avoid the experimental tuning of the model and reduce the computational load, a new model was proposed.

The proposed model was based on parallel-plate model (Equation (10)) [59]. In the parallel-plate model, Paschen's law is used (Equation (2)). As explained in Section 2.2.1, this equation does not consider how the temperature changes the air properties. As a result, it is not accurate at high temperatures. However, it is possible to apply Peek (Equation (6)) or Dunbar (Equation (7)) corrections to solve this issue. Thus, the use of these temperature correction methods in a parallel-plate model was proposed.

Firstly, it was necessary to adjust γ. In Figure 15, a comparison of the experimentally measured data (sample group C) and parallel-plate model, evaluated for different γ values proposed in the literature at ambient temperature, is depicted. $\gamma = 0.01$ is a well-known value for metallic electrodes, which was also used in insulated twisted pairs [63,69]. $\gamma = 0.001$ is the value used by [59] to develop the parallel-plate model (the one that best fits their experimental data). $\gamma = 0.0006$ was proposed by [62] for PAI overcoat samples, $\gamma = 0.00065$ was proposed for PI insulation by [73], and $\gamma = 0.0078$ was reported by [70] for epoxy resin. It can be seen that the γ values proposed for PAI and PI best fit the experimental results. The PDIV estimation in both cases does not differ, due to close γ values and the error for both being around 1%.

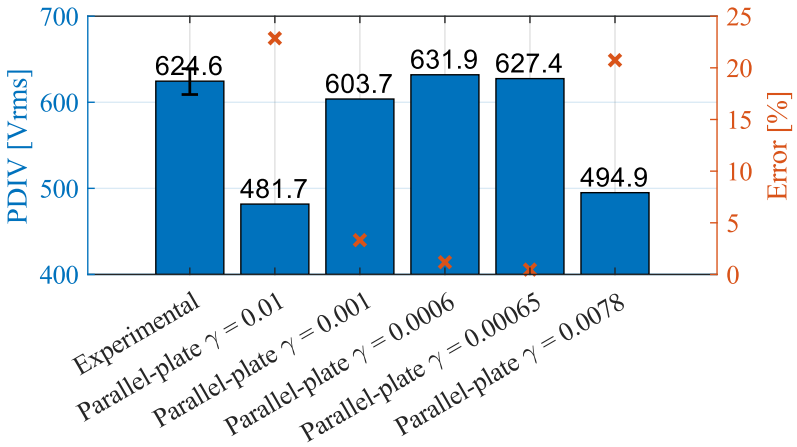

Figure 15. Comparison of experimental measurements and parallel-plate model for different γ values at room temperature (sample group C). Crosses represent the error.

Once γ was adjusted, the Peek and Dunbar corrections were applied to Equation (10). This way, the parallel-plate model was corrected as Equation (23) with Peek correction (based on Equations (2), (6), and (10)) and Equation (24) with Dunbar correction (based on Equations (2), (7) and (10)).

$$\mathrm{PDIV} = min\left[\frac{\frac{P_{new}}{P_{ref}}\frac{T_{ref}}{T_{new}}B\frac{P_{ref}\,d_{air}}{ln\left(\frac{AP_{ref}\,d_{air}}{k}\right)}}{d_{air}}\left(d_{air}+\frac{t_{ins1}}{\varepsilon_{r1}}+\ldots\right)\right] \tag{23}$$

$$\text{PDIV} = min\left[\frac{B\frac{P_{\text{ref}}\frac{T_{\text{ref}}}{T_{\text{new}}}d_{\text{air}}}{ln\left(\frac{AP_{\text{ref}}\frac{T_{\text{ref}}}{T_{\text{new}}}d_{\text{air}}}{k}\right)}}{d_{\text{air}}}\left(d_{\text{air}}+\frac{t_{\text{ins1}}}{\varepsilon_{\text{r1}}}+\ldots\right)\right] \tag{24}$$

where A and B are experimental constants and depend on the gas composition (for air: 11.25 $\text{Pa}^{-1}\text{m}^{-1}$ and 273.75 $\text{VPa}^{-1}\text{m}^{-1}$, respectively, [58]). d_{air} is the straight distance between surfaces. k is defined in Equation (3). P_{ref} and T_{ref} are the pressure and temperature at room conditions, respectively, and P_{new} and T_{new} are the pressure and temperature at which the PDIV is estimated, respectively. $t_{\text{ins}i}$ and ε_{ri} are the thickness and the relative permittivity of each insulation layer, respectively.

The results obtained using the correction of temperature using Equations (23) and (24) are illustrated in Figure 16 in comparison with the experimental measurements (sample group C). In this case, $\gamma = 0.00065$ was used, as defined by [73] for PI. In comparison with the results observed in Figure 12, using the correction of the Dunbar for the Paschen's curve, the maximum error developed by the model decreases from 25% to around 12%. On the contrary, the Peek Paschen's correction does not provide such good accuracy, as stated in [65,72].

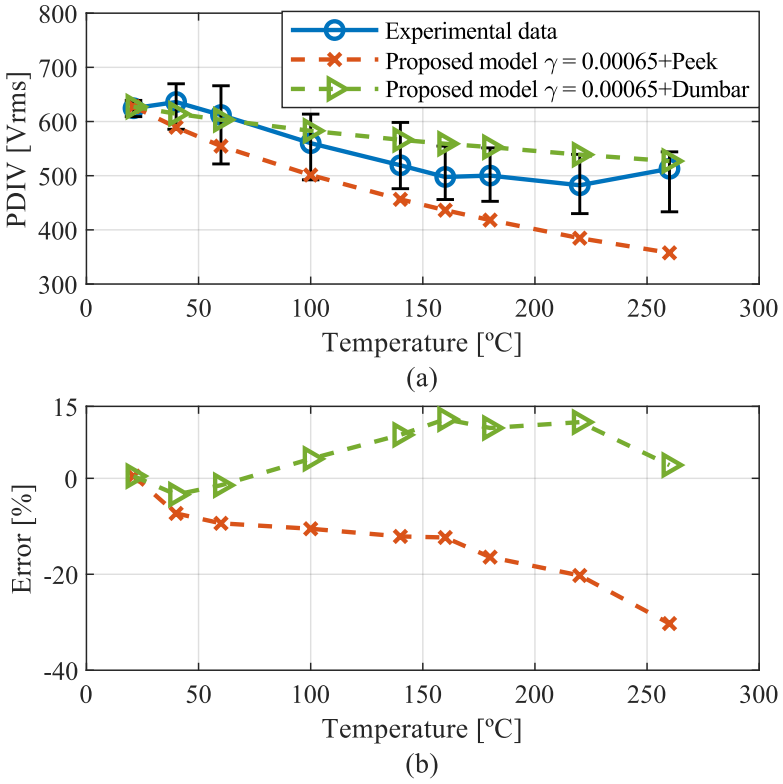

Figure 16. Comparison of experimental measurements and proposed new model for different temperatures (sample group C): (**a**) PDIV; (**b**) error.

Thus, it can be concluded that the proposed new model (Equation (24)) with the implementation of the Dunbar correction for Paschen's law can lead to a good estimation of the PDIV for different temperatures. The resulting error was in good agreement with that reported in [70] for the estimation of the PDIV using FEM and the corrected Paschen's curve with γ and Dunbar correction, where a maximum error of 11.15% was achieved. This way, the experiments and high computational load could be avoided.

4.2.6. Comparison of Models

The analytical and FEM-based models are compared in order to provide some guidelines regarding the selection of a suitable model for PDIV estimation at variable temperatures. The Dakin model [74], Lusuardi model [26], FEM and Paschen's law model [38,60,62,69], and the proposed model are compared. Among them, the Dakin model suggested in [74] can only consider the evolution of permittivity with the temperature, whereas the Lusuardi model [26] only considers the effect of air temperature and pressure. The FEM and Paschen's law model [38,60,62,69] and the new proposed model consider both the evolution of relative permittivity and air properties with temperature. It is necessary to specify that only the FEM and Paschen's law model, with the straight distance between wire surfaces, is represented in this comparison.

Figure 17 shows the comparison for sample group B. On the one hand, it is shown that the Dakin model, which is unique in that it does not consider the effect of temperature on the air properties, differs considerably from the experimental results. The other models all provide similar results. The Lusuardi model proposed by L. Lusuardi et al. [26] returns a slightly higher error, as a constant relative permittivity is considered. The FEM-based model [38,60,62,69] returns a much smaller error value. In all cases, at temperatures higher than 150 °C, the estimated values are not inside the measurement uncertainty range. Y. Kemari et al. [73] considered a similar case. In order to understand where this difference comes from, they analysed the γ estimation for different temperatures. They noticed that the γ value calculated for high temperatures did not considerably differ from the room temperature values. Therefore, they concluded that the difference could be due to the impact of the moisture, which is not considered in the models, or the uncertainty in the sample thickness and geometry changing with temperature.

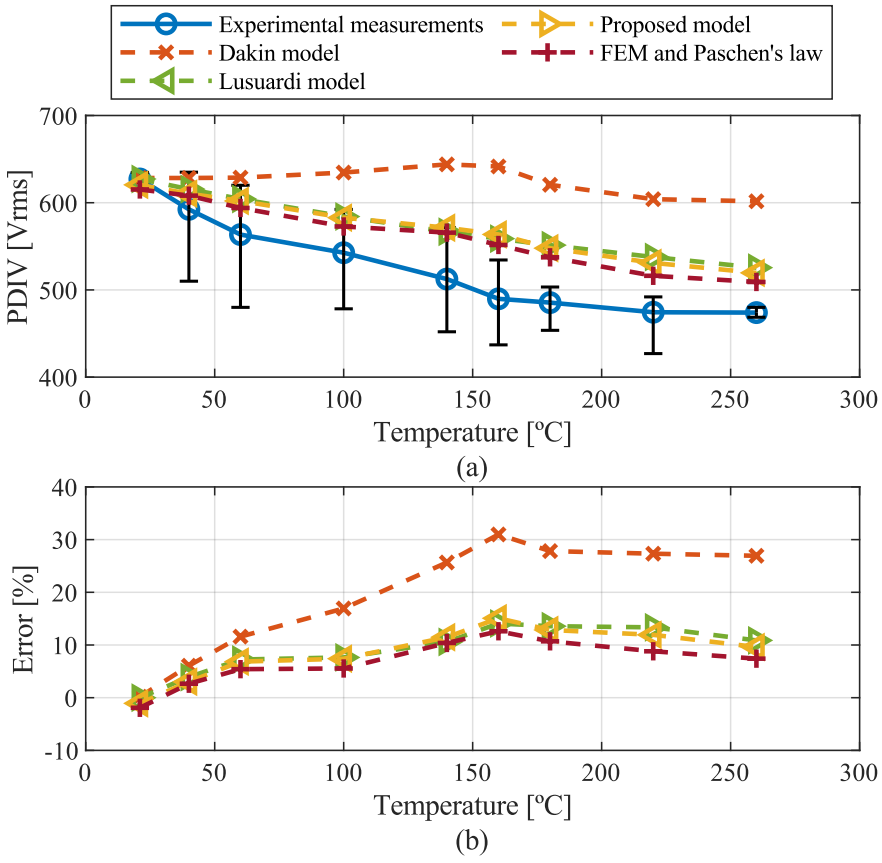

Figure 17. Comparison of PDIV models and experimental measurements for different temperatures (sample group B): (**a**) PDIV and (**b**) error.

Figure 18 illustrates the comparison for sample group C. Similar to sample group B, the Dakin model is not good enough to predict the PDIV at elevated temperatures. For the rest of the models, the difference between them is not appreciable. Compared to sample group B, the relative permittivity of group C is almost constant for the studied temperature range and, hence, similar results were obtained for these models.

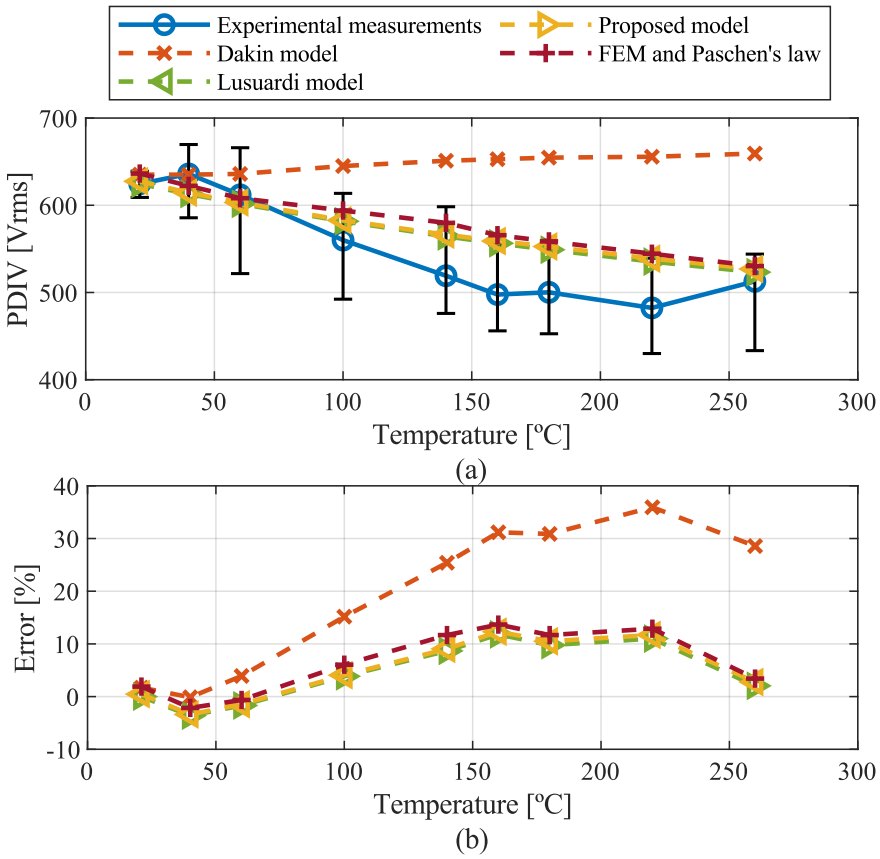

Figure 18. Comparison of PDIV models and experimental measurements for different temperatures (sample group C): (**a**) PDIV; (**b**) error.

5. Discussion

5.1. Variables Affecting PDIV

Starting with environmental conditions, there is a consensus that PDIV's dependency on pressure has a *U* shape, where the PDIV decreases and then increases with an increase in the pressure. In spite of the decreasing PDIV tendency with pressure being clear, the decrease perceived by L. Lusuardi et al. [26] and D. Meyer et al. [28] is slightly higher than that found by C. Abadie et al. [27] (Figure 1). This difference may result from the use of different insulation materials, which are not specified in the articles.

Moving on to relative humidity, at high voltage (>5300 V) there are two main mechanisms related to an increase in the humidity. On the one hand, there is the increase in the air breakdown strength and decrease in the PD activity surface. On the other hand, there is the increase in insulation bulk charge accumulation and relative and imaginary part of permittivity. At low RH values, the first mechanism is predominant and the PDIV increases until a peak value with the increase in RH. Then, the PDIV decreases due to the predominance of the second mechanism. At voltages lower than 3450 V, however, the second mechanism seems to be predominant in the whole range of RH. Still, some authors describe an inverse effect on the PDIV or even no effect of the RH on cleaned samples. Thus, further investigation is required.

For environmental conditions, all the authors in the literature review agree that an increase in temperature decreases the PDIV due to the air electric breakdown strength decrease and the change in the relative permittivity of the enamel. Air breakdown strength always decreases with temperature, decreasing the PDIV. The relative permittivity, conversely, can increase/decrease with temperature depending on the material and its effect on the PDIV can change. If the relative permittivity decreases, air and relative permittivity may affect the PDIV in opposite ways. In this article, we studied whether air properties or relative permittivity prevail in the PDIV. We concluded that changes in the air properties are the dominating factor affecting the PDIV. The relative permittivity should decrease by around 25% of the current value at 180 °C to neutralise the decreasing effect of the air breakdown strength on the PDIV. Hence, in spite of both air properties and relative permittivity being considered to evaluate how the PDIV changes with the temperature, the temperature always has an inverse effect on the PDIV.

For the electrical factors, the PDIV is not affected by the waveform (sinusoidal, square bipolar, or unipolar) and polarity but the peak-to-peak applied voltage value is the main factor to define the PDIV. Nevertheless, it is important to consider both the waveform and polarity in the case of consequent PDIV measurements, due to the charge accumulation (the memory effect). The authors agree that the frequency does not affect the PDIV as long as the permittivity of the insulation material does not depend on the tested frequency range. The negligible difference observed by Z. Wei et al. [47] (was that the PDIV changed by 6% at 1–10 kHz), which could be because the pulse width changes while the duty is maintained for different frequencies. According to [43], the pulse width could affect the PDIV. Frequency affects the RPDIV by the enhancement of free electron availability due to charge accumulation at frequencies below 10 kHz, decreasing the RPDIV while increasing the switching frequency. Additionally, the increase in overshoot average amplitude has an analogous effect on PD provability and, therefore, decreases the RPDIV at frequencies up to 75–100 kHZ. Over 100 kHz, the RPDIV tends to stabilise with the increase in frequency.

Regarding the rise time, when the PDIV is measured with high overshoot, the overshoot level and ringing are the major factors affecting the PDIV. The measurement of an accurate PDIV value is not possible, as the error is due to the overshoot, whether DC or peak voltage is considered as the PDIV. Nonetheless, it is noteworthy that, in [54], there is no effect at the peak PDIV for 56% overshoot (Figure 5). This difference from other studies could be related to the availability of the starting electron. The author of [46] explains that the higher PDIV resulting from high overshoots is due to the low probability of having a starting electron due to the short time above the inception level in each overshoot. Hence, the peak PDIV value is increased, as in [26,45]. Conversely, the author of [53] notes that, with high ringing (several oscillations/overshoots before achieving DC voltage), the increase in the average voltage (even maintaining peak voltage) increases the probability of starting the electron availability, as the inception level is surpassed several times. In this way, the PD provability increases and the PDIV decreases. As a consequence, the results [54] suggest that there is a high ringing in the used waveform. As the inception voltage is surpassed with a high starting electron probability, the peak PDIV would be defined by a similar value of inception voltage and the DC PDIV will be defined by a lower voltage level. It could be said that, for high ringing, a high overshoot affects the DC PDIV but not peak PDIV, as shown in [54]. However, this hypothesis cannot be verified as there is no information about waveform ringing in [54].

In cases where measurements are developed without overvoltage and avoiding charge accumulation, there is no consistent answer in the literature. Some conclude that there is no effect of rise time on the PDIV, whereas others observed a decrease in the PDIV when decreasing the rise time. Considering that the rise time does affect the PDIV, with a lower rise time, the initial electron generation starts faster, reaching the critical electron number earlier, so the PDIV can be defined by a lower applied voltage, as long as the inception voltage is overcome. Further study is still necessary.

To end with electrical variables, the influence of the pulse width on the PDIV is not clear. For high rise times, the effect of the pulse width appears to be negligible, as the critical initial electron number is reached during rising. For lower rise times, the authors of [43] stated that the pulse width decreased PDIV, whereas, in [57], it increased or did not change (depending on the voltage nonconducting duration).

The main difference between [43] and the rest of the mentioned studies [52,54,57] is that the pulse width is achieved from different conventions of switching frequency and duty rate. Consequently, the nonconducting duration could vary from the maximum to the minimum pulse width, affecting the PDIV results, as explained in [57]. For example, if a 100 kHz switching frequency and 0.2 duty ratio and 1 kHz switching frequency and 0.8 duty ratio are used to acquire 2 µs and 800 µs pulse widths, respectively, the nonconducting duration could vary from 8 to 200 µs. Hence, it could be rather difficult to distinguish whether the pulse width or the charge accumulation is influencing the PDIV. Nonetheless, the influence of the nonconducting duration cannot be distinguished, as there are no data [43].

Overall, it could be concluded that the effect of the pulse width cannot be studied independently of the rise time and duty. As far as we know, the effect of the pulse width considering the nonconduction duration has not been studied for a short pulse width with a short rise time. Further investigation is necessary to achieve more consistent conclusions in this area. A multifactorial study could be used to analyse the real effect of the waveform characteristics.

5.2. PDIV Estimation Models

Analytical, FEM-based, and probability-based models are collected in this article. This resulted in a summary where the used variables, considered changing variables, and the pros and cons of each model, are gathered. Within the models, two considered rise time and pulse width (group 1), whereas six considered environmental conditions, whether pressure, temperature, or both (group 2). This summary can help with the selection of the best model that fits some specific requirements.

In order to evaluate models from group 2 at high temperature, experiments were performed in a temperature range of 20–260 °C for two different enamel twisted pairs. To estimate the PDIV based on temperature evolution, the proposed new model offers the best compromise between accuracy and computational cost. The FEM-based models [38,60,62,69] require FEM software and a large amount of computation time. In the Lusuardi model [26], it is necessary to measure the PDIV at least at a reference temperature. Moreover, the relative permittivity must not vary with the temperature. In the proposed new model, the changes in the relative permittivity with the temperature can be considered and FEM analysis and experiments could be skipped. However, it is true that the correct definition of γ value is a key factor and could be difficult to define. If γ for a specific material is not defined in the bibliography, the experimental measurements might be necessary for its definition. This issue is presented in all models using Paschen's law.

It has to be mentioned that the models analysed in Figures 17 and 18 do not consider electrical waveform characteristics, such as overvoltage, pulse width, or rise time, which can influence the PDIV, as presented in Section 2.1. Despite their use for predicting the PDIV, when it is measured with a sinusoidal waveform, it is shown to be accurate (with different limitations regarding environmental conditions, depending on the model) and it is still not clear what their accuracy is in the estimation of PDIV in cases where waveforms with different characteristics are used. For instance, waveforms with overvoltage may be more difficult to predict. To consider these characteristics, the models proposed by Z. Wei et al. [43] and N. Hayakawa et al. [31] should be used. The former only considers the rise time and pulse width, whereas the latter considers overshoots as well. However, neither of them consider environmental conditions for twisted pair PDIV estimation. So, although the extended volume–time theory proposed by N. Hayakawa et al. [31] provides a good

basis to consider most relevant electrical waveform characteristics, it is necessary to develop more studies regarding the models considering both environmental and electrical variables.

6. Conclusions

In this paper, a thorough analysis of different electrical waveform factors and environmental conditions affecting PDIV was performed. In addition, different PDIV estimation models from the literature were reviewed identifying the pros and cons. Given the importance of temperature on the PDIV and the high temperature of the winding during operation (180 °C), several models were studied at high temperature. For that, the experiments were performed at the range of 20–260 °C. The advantages and disavantages of the Dakin, parallel-plate, Lusuard,i and FEM and Paschen's models were identified in comparison to the experiments. Based on the drawback of these models, a new model avoiding experiments and computational simulations is proposed. The proposed model is based on the parallel-plate model, where Dunbar correction was implemented in order to consider the effect of the temperature on air properties. The proposed model showed the best compromise between computational requirements and estimation accuracy at different temperature levels. Furthermore, the effect of permittivity was also considered.

Even though there is a general agreement regarding how variables such as pressure, temperature, waveform, and polarity or frequency affect the PDIV, further studies are necessary in terms of humidity, rise time, and pulse width. Independent analysis of the pulse width in the literature does not provide consistent results. Therefore, a multifactorial analysis of the rise time, pulse width, and duty is recommended, with and without overshoot waveforms.

Additionally, a model that is able to consider the overshoot and ringing resulting from WBG-based converters, where environmental conditions are also considered, is still necessary. The extended volume–time theory seems to be a good basis to consider different waveform characteristics, but the effect of environmental conditions should be added.

The present article can form a basis to continue developing the PDIV estimation models for turn-to-turn insulation systems. It provides an overview of the different factors affecting the PDIV, together with different models to estimate it. It also offers a simple PDIV estimation model considering the temperature evolution.

Author Contributions: Conceptualization, L.E.A., G.A. and A.E.; methodology, L.E.A., G.A. and A.E.; validation, L.E.A., G.A. and A.E.; formal analysis, L.E.A., G.A., A.E. and X.B.; investigation, L.E.A., G.A., A.E., G.U. and X.B.; data curation, L.E.A.; writing—original draft preparation, L.E.; writing—review and editing, L.E.A., G.A., A.E., G.U. and X.B.; supervision, G.A., A.E. and G.U.; project administration, G.A., A.E. and G.U.; funding acquisition, G.A., A.E. and G.U. All authors have read and agreed to the published version of the manuscript.

Funding: This research was funded by the ELKARTEK program of the Department of Economic development, Sustainability and Environment of the Basque Government grant number KK-2021/00044 and KK-2022/00073.

Institutional Review Board Statement: Not applicable.

Informed Consent Statement: Not applicable.

Data Availability Statement: The data presented in this study are available on request from the corresponding author.

Conflicts of Interest: The authors declare no conflict of interest.

Abbreviations

The following abbreviations are used in this manuscript:

EV	Electric Vehicle
RH	Relative Humidity
AC	Alternating Current
DC	Direct Current
PD	Partial Discharge
PDIV	Partial Discharge inception Voltage
RPDIV	Repetitive Partial Discharge inception Voltage
RP	Relative Permittivity
FEM	Finite Element Method

References

1. Commission, E. European Green Deal: Commission Proposes Transformation of EU Economy and Society to Meet Climate Ambitions. 2021. Available online: https://ec.europa.eu/commission/presscorner/detail/en/IP_21_3541 (accessed on 1 August 2022).
2. Laszlo, B. Introduction to the Fundamental Technologies of Power Density—Power Management—Technical Articles—TI E2E Support Forums. 2020. Available online: https://e2e.ti.com/blogs_/b/powerhouse/posts/introduction-to-the-fundamental-technologies-of-power-density (accessed on 1 August 2022).
3. Morya, A.K.; Gardner, M.C.; Anvari, B.; Liu, L.; Yepes, A.G.; Doval-Gandoy, J.; Toliyat, H.A. Wide Bandgap Devices in AC Electric Drives: Opportunities and Challenges. *IEEE Trans. Transp. Electrif.* **2019**, *5*, 3–20. [CrossRef]
4. Han, D.; Li, Y.; Sarlioglu, B. Analysis of SiC based power electronic inverters for high speed machines. In Proceedings of the 2015 IEEE Applied Power Electronics Conference and Exposition (APEC), Charlotte, NC, USA, 15–19 March 2015; pp. 304–310. [CrossRef]
5. Kumar, K.; Santra, S.B. Performance Analysis of a Three-Phase Propulsion Inverter for Electric Vehicles Using GaN Semiconductor Devices. *IEEE Trans. Ind. Appl.* **2018**, *54*, 6247–6257. [CrossRef]
6. Xu, Y.; Yuan, X.; Ye, F.; Wang, Z.; Zhang, Y.; Diab, M.; Zhou, W. Impact of High Switching Speed and High Switching Frequency of Wide-Bandgap Motor Drives on Electric Machines. *IEEE Access* **2021**, *9*, 82866–82880. [CrossRef]
7. Morya, A.; Toliyat, H.A. Insulation design for Wide Bandgap (WBG) device based voltage source converter fed motors. In Proceedings of the 2017 IEEE 5th Workshop on Wide Bandgap Power Devices and Applications (WiPDA), Albuquerque, NM, USA, 30 October–1 November 2017; pp. 74–79. [CrossRef]
8. Carlsson, A.; Josefsson, V.; Nategh, S.; Boglietti, A.; Arvidsson, R. Insulation System Design for 800 V Traction Motors Used in E-mobility Applications. In Proceedings of the 2022 International Conference on Electrical Machines (ICEM), Valencia, Spain, 5–8 September 2022; pp. 1321–1326. [CrossRef]
9. He, J.; Chen, H.; Katebi, R.; Weise, N.; Demerdash, N.A. Mitigation of uneven surge voltage stress on stator windings of induction motors fed by SiC-MOSFET-based adjustable speed drives. In Proceedings of the 2017 IEEE International Electric Machines and Drives Conference (IEMDC), Miami, FL, USA, 21–24 May 2017 pp. 1–7. [CrossRef]
10. *IEC 60034-18-41:2014*; Rotating Electrical Machines—Part 18-41: Partial Discharge Free Electrical Insulation Systems (Type I) Used in Rotating Electrical Machines Fed from Voltage Converters—Qualification and Quality Control Tests; IEC: Geneva, Switzerland, 2014.
11. Scott, M.J.; Brockman, J.; Hu, B.; Fu, L.; Xu, L.; Wang, J.; Darbali Zamora, R. Reflected wave phenomenon in motor drive systems using wide bandgap devices. In Proceedings of the 2014 IEEE Workshop on Wide Bandgap Power Devices and Applications, Knoxville, TN, USA, 13–15 October 2014 pp. 164–168. [CrossRef]
12. Selema, A.; Ibrahim, M.N.; Sergeant, P. Electrical Machines Winding Technology: Latest Advancements for Transportation Electrification. *Machines* **2022**, *10*, 563. [CrossRef]
13. Hemmati, R.; Wu, F.; El-Refaie, A. Survey of Insulation Systems in Electrical Machines. In Proceedings of the 2019 IEEE International Electric Machines & Drives Conference (IEMDC), San Diego, CA, USA, 12–15 May 2019; pp. 2069–2076. [CrossRef]
14. Cruz, J.d.S.; Fruett, F.; Lopes, R.d.R.; Takaki, F.L.; Tambascia, C.d.A.; de Lima, E.R.; Giesbrecht, M. Partial Discharges Monitoring for Electric Machines Diagnosis: A Review. *Energies* **2022**, *15*, 7966. [CrossRef]
15. He, J.; Li, C.; Jassal, A.; Thiagarajan, N.; Zhang, Y.; Prabhakaran, S.; Feliz, C.; Graham, J.; Kang, X. Multi-Domain Design Optimization of dv/dt Filter for SiC-Based Three-Phase Inverters in High-Frequency Motor-Drive Applications. In Proceedings of the 2018 IEEE Energy Conversion Congress and Exposition (ECCE), Portland, OR, USA, 23–27 September 2018; pp. 5215–5222. [CrossRef]
16. Montanari, G.C.; Seri, P. The effect of inverter characteristics on partial discharge and life behavior of wire insulation. *IEEE Electr. Insul. Mag.* **2018**, *34*, 32–39. [CrossRef]
17. Grau, V.; De Doncker, R.W. The Effects of Steep Voltage Slopes on Insulation Systems of Coil Windings caused by Next Generation Power Semiconductor Devices. In Proceedings of the 2019 IEEE Electrical Insulation Conference (EIC), Calgary, AB, Canada, 16–19 June 2019; pp. 26–29. [CrossRef]
18. Florkowski, M.; Florkowska, B.; Zydron, P. Partial Discharges in Insulating Systems of Low Voltage Electric Motors Fed by Power Electronics—Twisted-Pair Samples Evaluation. *Energies* **2019**, *12*, 768. [CrossRef]

19. Akram, S.; Wang, P.; Nazir, M.T.; Zhou, K.; Bhutta, M.S.; Hussain, H. Impact of impulse voltage frequency on the partial discharge characteristic of electric vehicles motor insulation. *Eng. Fail. Anal.* **2020**, *116*, 104767. [CrossRef]
20. Guastavino, F.; Dardano, A.; Ratto, A.; Torello, E. Electrical aging test on twisted pair specimens under different environmental conditions. In Proceedings of the Conference on Electrical Insulation and Dielectric Phenomena, CEIDP, Virginia Beach, VA, USA, 18–21 October 2009; pp. 81–84. [CrossRef]
21. Savin, S.; Ait-Amar, S.; Roger, D. Turn-to-turn capacitance variations correlated with PDIV for AC motors monitoring. *IEEE Trans. Dielectr. Electr. Insul.* **2013**, *20*, 34–41. [CrossRef]
22. Liu, X.; Zhang, T.; Bai, Y.; Ding, X.; Wang, Y. Effects of accelerated repetitive impulse voltage aging on performance of model stator insulation of wind turbine generator. *IEEE Trans. Dielectr. Electr. Insul.* **2014**, *21*, 1506–1515. [CrossRef]
23. Succi, R.; Han, T.; Cavallini, A. An Investigation on the Dielectric Properties of Thermally-Aged Kapton and its Capability to Withstand Partial Discharges. In Proceedings of the 2019 IEEE Conference on Electrical Insulation and Dielectric Phenomena (CEIDP), Richland, WA, USA, 20–23 October 2019; pp. 381–384. [CrossRef]
24. Guastavino, F.; Briano, L.; Gallesi, F.; Torello, E. Effect of Thermal Stress Over the Partial Discharge Inception Voltage on Twisted Pairs. In Proceedings of the 2020 IEEE Conference on Electrical Insulation and Dielectric Phenomena (CEIDP), East Rutherford, NJ, USA, 18–30 October 2020; pp. 366–368. [CrossRef]
25. Lehr, J.; Ron, P. *Electrical Breakdown in Gases*; John Wiley & Sons, Inc.: Hoboken, NJ, USA, 2017; pp. 369–438. [CrossRef]
26. Lusuardi, L.; Rumi, A.; Cavallini, A.; Barater, D.; Nuzzo, S. Partial Discharge Phenomena in Electrical Machines for the More Electrical Aircraft. Part II: Impact of Reduced Pressures and Wide Bandgap Devices. *IEEE Access* **2021**, *9*, 27485–27495. [CrossRef]
27. Abadie, C.; Billard, T.; Lebey, T. Partial Discharges in Motor Fed by Inverter: From Detection to Winding Configuration. *IEEE Trans. Ind. Appl.* **2019**, *55*, 1332–1341. [CrossRef]
28. Meyer, D.R.; Cavallini, A.; lusuardi, L.; Barater, D.; Pietrini, G.; Soldati, A. Influence of impulse voltage repetition frequency on RPDIV in partial vacuum. *IEEE Trans. Dielectr. Electr. Insul.* **2018**, *25*, 873–882. [CrossRef]
29. Fenger, M.; Stone, G.C. Investigations into the effect of humidity on stator winding partial discharges. *IEEE Trans. Dielectr. Electr. Insul.* **2005**, *12*, 341–346. [CrossRef]
30. Radmilović-Radjenović, M.; Radjenović, B.; Nikitović, Ž.; Matejčik, Š.; Klas, M. The humidity effect on the breakdown voltage characteristics and the transport parameters of air. *Nucl. Instruments Methods Phys. Res. Sect. B: Beam Interact. Mater. Atoms* **2012**, *279*, 103–105. [CrossRef]
31. Hayakawa, N.; Shimizu, F.; Okubo, H. Estimation of partial discharge inception voltage of magnet wires under inverter surge voltage by volume-time theory. *IEEE Trans. Dielectr. Electr. Insul.* **2012**, *19*, 550–557. [CrossRef]
32. Fabiani, D.; Montanari, G.C.; Testa, L.; Schifani, R.; Guastavino, F.; Bellucci, F.; Deorsola, F. Effect of water adsorption on the dielectric properties of polymer nanocomposites. In Proceedings of the International Symposium on Electrical Insulating Materials, Yokkaichi, Japan, 7–11 September 2008; pp. 510–513. [CrossRef]
33. Fabiani, D.; Montanari, G.C.; Cavallini, A.; Mazzanti, G. Relation between space charge accumulation and partial discharge activity in enameled wires under PWM-like voltage waveforms. *IEEE Trans. Dielectr. Electr. Insul.* **2004**, *11*, 393–405. [CrossRef]
34. Han, T.; Cavallini, A. Dielectric properties and partial discharge endurance of thermally aged nano-structured polyimide. *IEEE Electr. Insul. Mag.* **2020**, *36*, 39–46. [CrossRef]
35. Kikuchi, Y.; Murata, T.; Fukumoto, N.; Nagata, M.; Wakimoto, Y.; Yoshimitsu, T. Investigation of partial discharge with twisted enameled wires in atmospheric humid air by optical emission spectroscopy. *IEEE Trans. Dielectr. Electr. Insul.* **2010**, *17*, 839–845. [CrossRef]
36. Kimura, K.; Hikita, M.; Hayakawa, N.; Nagata, M.; Kadowaki, K.; Murakami, Y. Round-robin test on repetitive PD inception voltage of twisted-pairs. In Proceedings of the Conference on Electrical Insulation and Dielectric Phenomena, CEIDP, West Lafayette, IN, USA, 17–20 October 2010; pp. 5–8. [CrossRef]
37. Matsumoto, S.; Nam, N.N.; Nagaba, D.; Ogiya, T. Partial discharge characteristics of twisted magnet wire under high frequency AC voltage. In Proceedings of the International Symposium on Electrical Insulating Materials, Niigata, Japan, 1–5 June 2014; pp. 57–60. [CrossRef]
38. Muto, D.; Oya, M.; Aoi, T.; Ueno, T. A study on partial discharge phenomena of winding wires. *Furukawa Rev.* **2014**, *45*, 13–21.
39. Hassan, W.; Hussain, G.A.; Mahmood, F.; Amin, S.; Lehtonen, M. Effects of Environmental Factors on Partial Discharge Activity and Estimation of Insulation Lifetime in Electrical Machines. *IEEE Access* **2020**, *8*, 108491–108502. [CrossRef]
40. He, J.; Wu, G.; Gao, B.; Wu, J. Study on aging characteristics for inverter-fed traction motor inter-turn insulation based on analysis of dielectric characteristic parameters. In Proceedings of the Conference on Electrical Insulation and Dielectric Phenomena, CEIDP, Vancouver, BC, Canada, 14–17 October 2007; pp. 81–84. [CrossRef]
41. Zenda, Y.; Takenouchi, S.; Kozako, M.; Hikita, M.; Okamoto, T.; Jintong, S.; Izumi, A.; Karasawa, K. Effect of Temperature on RPDIV of Enamel Twisted Pair under Repetitive Impulse Voltage Application with Different Rise Time. In Proceedings of the Conference on Electrical Insulation and Dielectric Phenomena, CEIDP, Vancouver, BC, Canada, 12–15 December 2021; pp. 603–606. [CrossRef]
42. Aakre, T.G.; Ildstad, E.; Hvidsten, S. Partial discharge inception voltage of voids enclosed in epoxy/mica versus voltage frequency and temperature. *IEEE Trans. Dielectr. Electr. Insul.* **2020**, *27*, 214–221. [CrossRef]
43. Wei, Z.; You, H.; Fu, P. Twisted Pairs Under Single Voltage Pulses Generated by Silicon-Carbide Devices. *IEEE Trans. Transp. Electrif.* **2022**, *8*, 1674–1683. [CrossRef]

44. Montanari, G.C.; Seri, P. About the Definition of PDIV and RPDIV in Designing Insulation Systems for Rotating Machines Controlled by Inverters. In Proceedings of the 2018 IEEE Electrical Insulation Conference (EIC), San Antonio, TX, USA, 17–20 June 2018; pp. 554–557. [CrossRef]
45. Wang, P.; Zhou, W.; Wang, K.; Li, J.; Zhou, Q.; Lei, Y. Comparison of PD characteristics for inverter-fed motor insulation under inusoidal and repetitive square wave voltage conditions. *Gaodianya Jishu/High Volt. Eng.* **2016**, *42*, 3895–3900. [CrossRef]
46. Rumi, A.; Cavallini, A.; lusuardi, L. Impact of WBG Converter Voltage Rise-Time and Switching Frequency on the PDIV of Twisted Pairs. In Proceedings of the 2020 IEEE 3rd International Conference on Dielectrics, ICD 2020, Valencia, Spain, 5–31 July 2020; pp. 902–905. [CrossRef]
47. Wei, Z.; You, H.; Hu, B.; Na, R.; Wang, J. Partial Discharge Behavior on Twisted Pair under Ultra-short Rise Time Square-wave Excitations. In Proceedings of the 2019 IEEE Electrical Insulation Conference (EIC), Calgary, AB, Canada, 16–19 June 2019; pp. 493–496. [CrossRef]
48. Wang, P.; Cavallini, A.; Montanari, G.C. The influence of square wave voltage duty cycle on PD behavior. In Proceedings of the Conference on Electrical Insulation and Dielectric Phenomena, CEIDP, Ann Arbor, MI, USA, 18–21 October 2015; pp. 338–341. [CrossRef]
49. Wang, P.; Yang, N.; Zheng, C.; Li, Y. Effect of repetitive impulsive and square wave voltage frequency on partial discharge features. In Proceedings of the IEEE International Conference on Properties and Applications of Dielectric Materials, Xi'an, China, 20–24 May 2018; pp. 152–155. [CrossRef]
50. Wang, P.; Cavallini, A.; Montanari, G.C. The influence of impulsive voltage frequency on PD features in turn insulation of inverter-fed motors. In Proceedings of the 2014 IEEE Conference on Electrical Insulation and Dielectric Phenomena, CEIDP 2014, Des Moines, IA, USA, 19–22 October 2014; pp. 35–38. [CrossRef]
51. Pan, C.; Wu, K.; Chen, G.; Gao, Y.; Florkowski, M.; Lv, Z.; Tang, J. Understanding Partial Discharge Behavior from the Memory Effect Induced by Residual Charges: A Review. *IEEE Trans. Dielectr. Electr. Insul.* **2020**, *27*, 1951–1965. [CrossRef]
52. Cavallini, A.; Lindell, E.; Montanari, G.C.; Tozzi, M. Inception of partial discharges under repetitive square voltages: Effect of voltage waveform and repetition rate on PDIV and RPDIV. In Proceedings of the 2010 Annual Report Conference on Electrical Insulation and Dielectic Phenomena, West Lafayette, IN, USA, 17–20 October 2010; pp. 1–4. [CrossRef]
53. lusuardi, L.; Cavallini, A.; Degano, M. The impact of impulsive voltage waveforms on the electrical insulation of actuators for more electrical aircraft (MEA). In Proceedings of the IECON 2017—43rd Annual Conference of the IEEE Industrial Electronics Society, Beijing, China, 29 October–1 November 2017; pp. 4414–4418. [CrossRef]
54. Naderiallaf, H.; Giangrande, P.; Galea, M. Investigating the Effect of Waveform Characteristics on PDEV, PDIV and RPDIV for Glass Fibre Insulated Wire. In Proceedings of the 2022 International Conference on Electrical Machines (ICEM), Valencia, Spain, 5–8 September 2022; pp. 1327–1333. [CrossRef]
55. Hu, B.; Wei, Z.; You, H.; Na, R.; Liu, R.; Xiong, H.; Fu, P.; Zhang, J.; Wang, J. A Partial Discharge Study of Medium-Voltage Motor Winding Insulation Under Two-Level Voltage Pulses With High Dv/Dt. *IEEE Open J. Power Electron.* **2021**, *2*, 225–235. [CrossRef]
56. Fu, P.; Zhao, Z.; Li, X.; Cui, X.; Yang, Z. The role of time-lag in the surface discharge inception under positive repetitive pulse voltage. *Phys. Plasmas* **2018**, *25*, 093518. [CrossRef]
57. Benmamas, L.; Teste, P.; Odic, E.; Krebs, G.; Hamiti, T. Contribution to the analysis of PWM inverter parameters influence on the partial discharge inception voltage. *IEEE Trans. Dielectr. Electr. Insul.* **2019**, *26*, 146–152. [CrossRef]
58. Husain, E.; Nema, R.S. Analysis of Paschen Curves for Air, N2 and SF6 Using the Townsend Breakdown Equation. *IEEE Trans. Electr. Insul.* **1982**, *EI-17*, 350–353. [CrossRef]
59. Szczepanski, M.; Fetouhi, L.; Sabatou, M.; Dreuilhe, S.; Pin, S.; Van de Steen, C.; Belijar, G. How does PDIV change during isothermal aging of magnet wire. In Proceedings of the 2022 IEEE Electrical Insulation Conference (EIC), Knoxville, TN, USA, 19–23 June 2022; pp. 266–271. [CrossRef]
60. Madonna, V.; Giangrande, P.; Zhao, W.; Buticchi, G.; Zhang, H.; Gerada, C.; Galea, M. Reliability vs. Performances of Electrical Machines: Partial Discharges Issue. In Proceedings of the 2019 IEEE Workshop on Electrical Machines Design, Control and Diagnosis (WEMDCD), Athens, Greece, 22–23 April 2019; Volume 1, pp. 77–82. [CrossRef]
61. Driendl, N.; Pauli, F.; Hameyer, K. Modeling of Partial Discharge Processes in Winding Insulation of Low-Voltage Electrical Machines Supplied by High du/dt Inverters. In Proceedings of the IECON 2019—45th Annual Conference of the IEEE Industrial Electronics Society, Lisbon, Portugal, 14–17 October 2019; Volume 1, pp. 7102–7107. [CrossRef]
62. Collin, P.; Malec, D.; Lefevre, Y. About the relevance of using Paschen's criterion for partial discharges inception voltage (PDIV) estimation when designing the electrical insulation system of inverter fed motors. In Proceedings of the 2019 IEEE Electrical Insulation Conference (EIC), Calgary, AB, Canada, 16–19 June 2019; pp. 513–516. [CrossRef]
63. Duchesne, S.; Parent, G.; Moenecley, J.; Roger, D. Prediction of PDIV in motor coils using finite element method. In Proceedings of the 2016 IEEE International Conference on Dielectrics (ICD), Montpellier, France, 3–7 July 2016; Volume 2, pp. 638–641. [CrossRef]
64. Nakaya, H.; Kozako, M.; Hikita, M.; Ohya, M.; Muto, D.; Tomizawa, K. Partial discharge inception voltage of enamel twisted-pair samples with several laminated insulation layers. In Proceedings of the 2013 Annual Report Conference on Electrical Insulation and Dielectric Phenomena, Chenzhen, China, 20–23 October 2013; pp. 1270–1273. [CrossRef]
65. Sili, E.; Cambronne, J.P. A New Empirical Expression of the Breakdown Voltage for Combined Variations of Temperature and Pressure. *Int. J. Aerosp. Mech. Eng.* **2012**, *6*, 611–616.

66. Chalise, S.R.; Grzybowski, S.; Taylor, C.D. Accelerated electrical degradation of machine winding insulation. In Proceedings of the 41st North American Power Symposium, Starkville, MS, USA, 4–6 October 2009; pp. 1–6. [CrossRef]
67. Okubo, H.; Hayakawa, N.; Montanari, G.C. Technical Development on Partial Discharge Measurement and Electrical Insulation Techniques for Low Voltage Motors Driven by Voltage Inverters. *IEEE Trans. Dielectr. Electr. Insul.* **2007**, *14*, 1516–1530. [CrossRef]
68. Hayakawa, N.; Okubo, H. Partial discharge characteristics of inverter-fed motor coil samples under ac and surge voltage conditions. *IEEE Electr. Insul. Mag.* **2005**, *21*, 5–10. [CrossRef]
69. Benmamas, L.; Teste, P.; Krebs, G.; Odic, E.; Vangraefschepe, F.; Hamiti, T. Contribution to partial discharge analysis in inverter-fed motor windings for automotive application. In Proceedings of the 2017 IEEE Electrical Insulation Conference (EIC), Baltimore, MD, USA, 11–14 June 2017; pp. 348–351. [CrossRef]
70. Gómez de la Calle, M.; Martínez-tarifa, J.M.; Member, S.; Manuel, Á.; Solanilla, G.; Robles, G.; Member, S. Uncertainty Sources in the Estimation of the Partial Discharge Inception Voltage in Turn-to-Turn Insulation Systems. *IEEE Access* **2020**, *8*, 157510–157519. [CrossRef]
71. Lusuardi, L.; Cavallini, A.; Calle, M.G.D.; Robles, G. Insulation Design of Low Voltage Electrical Motors Fed by PWM Inverters. *IEEE Electr. Insul. Mag.* **2019**, *35*, 7–15. [CrossRef]
72. Sili, E.; Koliatene, F.; Cambronne, J.P. Pressure and temperature effects on the paschen curve. In Proceedings of the Conference on Electrical Insulation and Dielectric Phenomena, CEIDP, Cancun, Mexico, 16–19 October 2011; pp. 464–467. [CrossRef]
73. Kemari, Y.; Steen, C.V.d.; Belijar, G.; Laudebat, L.; Diaham, S.; Valdez-Nava, Z.; Abadie, C. A Townsend's secondary ionization coefficient estimation method for partial discharge inception voltage prediction for insulating polymers. In Proceedings of the 2022 IEEE 4th International Conference on Dielectrics (ICD), Palermo, Italy, 3–7 July 2022; pp. 226–229. [CrossRef]
74. Dakin, T.W.; Philofsky, H.M.; Divens, W.C. Effect of electric discharges on the breakdown of solid insulation. *Trans. Am. Inst. Electr. Eng. Part I Commun. Electron.* **1954**, *73*, 155–162. [CrossRef]
75. Halleck, M.C. Calculation of Corona-Starting Voltage in Air-Solid Dielectric Systems. *Trans. Am. Inst. Electr. Eng. Part III Power Appar. Syst.* **1956**, *75*, 211–216. [CrossRef]
76. Gómez, M.; Calle, D. Partial Discharge Inception Voltage in Turn-To-Turn Insulation Systems: Modelling and Uncertainties. Ph.D. Thesis, Universidad Carlos III de Madrid, Getafe, Spain, 2021.
77. Lau, Y.Y.; Liu, Y.; Parker, R.K. Electron emission: From the Fowler-Nordheim relation to the Child-Langmuir law. *Phys. Plasmas* **1994**, *1*, 2082–2085. [CrossRef]
78. Ito, K.; Shibata, T.; Kawasaki, T. Development of High Voltage Wire for New Structure Motor in Full Hybrid Vehicle. *SAE Int. J. Altern. Powertrains* **2016**, *5*, 272–277. [CrossRef]
79. En, N.E.; Iec, N.I.; Une-en, N.; Goi, M.; Politeknikoa, E. *UNE-EN 60317-0-1*; Especificaciones para tipos particulares de hilos para bobinas electromagnéticas Parte 0-1: Requisitos generales Hilo de cobre de sección circular esmaltado. UNE: Madrid, Spain, 2014.
80. *UNE-EN IEC 60172*; Norma Española Temperatura de los Hilos Esmaltados y Recubiertos con Cinta para Bobinas Electromagnéticas. UNE: Madrid, Spain, 2021.
81. *UNE-EN 60270:2002/A1*; Técnicas de Ensayo en Alta Tensión Medidas. Medidas de las Descargas Parciales. UNE: Madrid, Spain, 2016.
82. Real Decreto 178/2021 de 23 de Marzo, por el que se Modifica el Real Decreto 1027/2007, de 20 de Julio, por el que se Aprueba el Reglamento de Instalaciones Térmicas en los Edificios. Available online: https://www.boe.es/eli/es/rd/2021/03/23/178 (accessed on 6 February 2023).
83. Guastavino, F.; Gianoglio, C.; Torello, E.; Ferraris, M.; Gianelli, W. Electrical Aging Tests on Conventional and Nanofilled Impregnation Resins. In Proceedings of the Conference on Electrical Insulation and Dielectric Phenomena, CEIDP, Cancun, Mexico, 21–24 October 2018; pp. 156–158. [CrossRef]
84. Park, J.; An, J.; Han, K.; Choi, H.S.; Seouk Park, I. Enhancement of cooling performance in traction motor of electric vehicle using direct slot cooling method. *Appl. Therm. Eng.* **2022**, *217*, 119082. .: 10.1016/j.applthermaleng.2022.119082. [CrossRef]
85. *UNE-EN IEC 60317-0-2*; Norma Española Bobinas Electromagnéticas Parte 0-2: Requisitos Generales Hilo de Cobre de Sección Rectangular Esmaltado. UNE: Madrid, Spain, 2021.